



HAL
open science

Instability of 2,2-di(pyridin-2-yl)acetic acid. Tautomerization decarboxylation

Piotr Borowski, Ryszard Gawinecki, Anna Milaczewska, Agnieszka Skotnicka,
Krzysztof Woliński, Agnieszka Brzyska

► **To cite this version:**

Piotr Borowski, Ryszard Gawinecki, Anna Milaczewska, Agnieszka Skotnicka, Krzysztof Woliński, et al.. Instability of 2,2-di(pyridin-2-yl)acetic acid. Tautomerization decarboxylation. *Journal of Molecular Modeling*, 2010, 17 (4), pp.857-868. 10.1007/s00894-010-0780-y . hal-00605261

HAL Id: hal-00605261

<https://hal.science/hal-00605261>

Submitted on 1 Jul 2011

HAL is a multi-disciplinary open access archive for the deposit and dissemination of scientific research documents, whether they are published or not. The documents may come from teaching and research institutions in France or abroad, or from public or private research centers.

L'archive ouverte pluridisciplinaire **HAL**, est destinée au dépôt et à la diffusion de documents scientifiques de niveau recherche, publiés ou non, émanant des établissements d'enseignement et de recherche français ou étrangers, des laboratoires publics ou privés.

Editorial Manager(tm) for Journal of Molecular Modeling
Manuscript Draft

Manuscript Number: JMM01310R1

Title: Instability of 2,2-di(pyridin-2-yl)acetic acid. Tautomerization versus decarboxylation

Article Type: Original paper

Keywords: Carboxylic acids, decarboxylation, tautomerization, reaction path, transition states, DFT calculations

Corresponding Author: Prof. Ryszard Gawinecki,

Corresponding Author's Institution:

First Author: Ryszard Gawinecki

Order of Authors: Ryszard Gawinecki; Piotr Borowski, Doctor; Anna Miłaczewska; Agnieszka Skotnicka, Doctor; Krzysztof Woliński, Professor; Agnieszka Brzyska

Abstract: The DFT calculations at the B3LYP level with 6-311G** basis set were carried out in order to reveal whether tautomerization or decarboxylation is responsible for the instability of 2,2-di(pyridin-2-yl)acetic (DPA) and 1,8-diazafluorene-9-carboxylic (DAF) acids. The carboxyl protons in both compounds are involved in the intramolecular hydrogen bonds (the pyridine nitrogen atoms are the hydrogen bond acceptors). Although formation of two intramolecular OH...N hydrogen bonds in the enols of both carboxylic acids enables effective electron delocalization within the quasi rings ($\cdots\text{H}\ddot{\text{O}}\text{C}=\ddot{\text{C}}=\text{N}$), only ene-1,1-diol of DAF has somewhat lower energy than DAF itself (ΔE is ca 7 kcal/mol). DPA and its enediol have comparable energies. Migration of the methine proton towards the carbonyl oxygen atom (to form enediols) requires overstepping the energy barriers of 55-57 kcal/mol for both DPA and DAF. The enaminone tautomers of the acids, formed by migration of this proton towards the pyridine nitrogen atom, are thermodynamically somewhat more stable than the respective enediols. The energy barriers of these processes are equal to ca 44 and 62 kcal/mol for DPA and DAF, respectively. Thus, such tautomerization of the acids is not likely to proceed. On the other hand, the distinct energetic effects (ca 15 kcal/mol) favour decarboxylation. This process involves formation of (E)-2-(pyridin-2(1H)-ylidenemethyl)pyridine and its cyclic analogue followed by their tautomerization to (dipyridin-2-yl)methane and 1,8-diazafluorene, respectively. Although the later compound was found to be somewhat thermodynamically more stable, kinetic control of tautomerization of the former is more distinct.

Response to Reviewers: Reply to the reviewers' comments:

Reviewer #1: The authors study, by employing DFT calculations, the processes of tautomerization and decarboxylation in two heterocycle-containing carboxylic acids. They have convincingly shown that the tautomerization of the acids is not likely and that the spontaneous decarboxylation is responsible for the instability of the reactant molecules, thus providing clues for the failed attempts by the group to synthesize the target compounds. The calculations are carefully done and results are sound. The methodology and level of DFT calculations are adequate. The manuscript is well structured and clearly written. However, I found the paper to be quite narrow in scope and thus, probably, of limited interest to the general audience of the journal.

Therefore, I think the paper would benefit if the authors elaborate more on the specific (medicinal) properties of these compounds (in the Introduction section), and draw more general conclusions about the chemical behavior of this class of molecules by contrasting the findings of the paper with those obtained for other similar systems (in the Conclusion section). One minor thing: misprint on p.3 (bottom): Fig. 11 should be Fig. 5.

2,2-Di(pyridin-2-yl)acetic acid and its cyclic analogue are supposed to be unstable compounds. We found DFT procedure to be very helpful to show what is the reason of this instability. Susceptibility of these compounds to undergo tautomeric rearrangements and decarboxylation are the only properties discussed in our paper (no other features of unstable compounds can be studied: they decompose during the measurement). On the other hand, explanation what are the products the labile compounds are transformed to, would be very helpful to other chemists trying to use them. Despite their instability, 2,2-di(pyridin-2-yl)acetic acids may appear as the intermediates in numerous (bio)chemical processes. Conclusions of the present paper may also refer to other substituted acetic acids (and their homologues) that carry electronegative heteroatoms in the gamma positions, such as diacylacetic acids and their derivatives (to be also known as unstable compounds). „Fig. 11" at the former p. 3 (bottom) is now changed to „Fig. 5". New fragments added in the text are in yellow.

Reviewer #2: This is a well written manuscript reporting theoretical study undertaken with the hope to clarify the reasons why the title compound is unstable. My major concern is about the very high barriers for TS1 and TS4, both of which are connected with transition states featuring 4-membered rings. The presence of such strained rings in TS is probably a major reason for the high activation barriers. If the hydrogen atom transfers could take place between two molecules of species 1 or 4, then the strained rings would be avoided in the transition states.

For example, b3lyp/6-311G**//b3lyp/6-31G calculations for 4a dimer shows that the activation energy (no ZPE included) for transformation into 5a dimer is only 17.9 kcal/mol, which is much lower than the reported value of 42.4 kcal/mol. Thus, I strongly recommend the Authors consider bimolecular reactions for steps 1 -> 2 and 4 -> 5 in the revised manuscript.

below are the coordinates (in Angstroms) for structures optimized by the Reviewer:

4a dimer

E b3lyp/6-311G** = -1069.61126123806

N	1.5489423635	2.2103437928	0.0455595610
C	1.5228968224	3.5556514313	-0.2240522151
C	0.4963869124	4.1045571620	-0.9394326169
C	-0.5622156284	3.2385064103	-1.3636926546
C	-0.5405795297	1.8962798487	-1.0850908377
C	0.5664411058	1.2980757148	-0.3762769669
H	2.3511118551	4.1288238983	0.1722882554
H	0.4828104687	5.1635795051	-1.1590887690
H	-1.3983940713	3.6551519128	-1.9159273117
H	-1.3337877585	1.2245031160	-1.3801122659
C	0.7500210355	-0.0506219493	-0.0880825981
H	2.2708453672	1.8667532029	0.6722754743

H	1.7290013927	-0.3370457624	0.2900474796
C	-0.1456695924	-1.1548150229	-0.3453310744
N	-1.4184556957	-0.9296684046	-0.8037084202
C	-2.2383568777	-1.9813915886	-1.0072949556
C	-1.8734313328	-3.3078294941	-0.7744540705
C	-0.5714273749	-3.5534586989	-0.3078939809
C	0.2906542733	-2.4851261774	-0.0947053257
H	-3.2323150053	-1.7368673381	-1.3713778942
H	-2.5747762228	-4.1152425677	-0.9500169292
H	-0.2382091704	-4.5687797044	-0.1161076417
H	1.3012617569	-2.6550470943	0.2633784216
N	0.3376712996	0.8034312285	3.0558327366
C	-0.9170243469	1.0116389258	3.5677751078
C	-1.0980153740	1.7729882988	4.6887884738
C	0.0600473634	2.3630324167	5.2895113735
C	1.3136559749	2.1626154419	4.7713627143
C	1.5176945074	1.3263507024	3.6107670622
H	-1.7269866449	0.5448611687	3.0217590208
H	-2.0883087407	1.9303119106	5.0947383488
H	-0.0587286626	2.9819553577	6.1732443139
H	2.2020107911	2.6031186792	5.2011911660
C	2.7320629442	0.9902700273	3.0219977070
H	0.4121193882	0.2935234023	2.1757359941
H	2.7004946392	0.2225887934	2.2520835821
C	4.0566718166	1.4284398438	3.3873484088
N	4.2364872761	2.3689067360	4.3702267501
C	5.4875912221	2.7644961941	4.6808401856
C	6.6358086325	2.2767782197	4.0559899374
C	6.4683883117	1.3111522536	3.0490739429
C	5.1885872679	0.8872079634	2.7149461011
H	5.5608380018	3.5091730180	5.4687287977
H	7.6183189518	2.6322657729	4.3440906266
H	7.3308556772	0.8964217289	2.5360164329
H	5.0404805288	0.1384322151	1.9424517596

TS

E b3lyp/6-311G** = -1069.58268906124

N	1.029760	2.499823	0.196416
C	0.902234	3.806808	-0.148924
C	-0.032480	4.188451	-1.090126
C	-0.854096	3.187289	-1.649989
C	-0.716237	1.857204	-1.274088
C	0.271834	1.480326	-0.333775
H	1.556518	4.496023	0.369511
H	-0.135028	5.228706	-1.370150
H	-1.606676	3.458596	-2.383014
H	-1.355938	1.075639	-1.658233
C	0.556169	0.145688	0.198638
H	1.678617	2.263432	1.016601
H	1.635981	-0.033463	0.236056
C	-0.159262	-1.066562	-0.264626
N	-1.402322	-0.965776	-0.810369

C	-2.063882	-2.094006	-1.154624
C	-1.542315	-3.374220	-0.976185
C	-0.260718	-3.488670	-0.417340
C	0.433504	-2.335011	-0.063822
H	-3.048683	-1.948424	-1.588002
H	-2.113687	-4.248918	-1.264973
H	0.188163	-4.464803	-0.263390
H	1.425017	-2.398507	0.372326
N	0.262923	0.704985	2.844894
C	-0.937857	0.533198	3.447956
C	-1.344524	1.293667	4.531259
C	-0.466144	2.307839	4.979605
C	0.761352	2.500248	4.372231
C	1.174061	1.653983	3.293616
H	-1.575166	-0.231585	3.013537
H	-2.307831	1.126335	4.997716
H	-0.756302	2.942935	5.811809
H	1.442062	3.282004	4.679416
C	2.430491	1.708722	2.615628
H	0.376600	0.284497	1.497412
H	2.727772	0.779246	2.133267
C	3.505715	2.645336	2.826446
N	3.283354	3.834166	3.484013
C	4.302894	4.707548	3.627734
C	5.591108	4.494690	3.138722
C	5.835252	3.284767	2.462931
C	4.807111	2.366497	2.309026
H	4.060631	5.622291	4.163530
H	6.370999	5.233878	3.282137
H	6.824293	3.065115	2.070622
H	4.981536	1.422917	1.800161

We would like to thank the reviewer for his/her valuable comments. We admit, we were not considering the bimolecular mechanisms from the very beginning. This was definitely the point worth further investigations. The reaction like $(4a)_2 \rightarrow 2\ 5a$ involves the proton transfer between the heteroatom (nitrogen, in this case) and the carbon atom. Indeed, we found the stable $(4a)_2$ dimer at the B3LYP level, just as the reviewer. The counterpoise (CP) corrected value of the binding energy turned out to be somewhat above 4 kcal/mol. We also found the transition state for the N1(A)...H9(A)...C7(B) proton transfer (A and B denote the different molecules of a dimer). The energy barrier, being close to 20 kcal/mol, was lower than that found for the unimolecular mechanism. Similar calculations were also carried out in the case of b-type systems (DAF), and the conclusions were basically the same as in the case of DPA; all data are now reported in the revised manuscript. However, in the meantime, we recalled the calculations we carried out before on systems interacting via the dispersive-type forces, the forces that may play a crucial role in the case of two 4a molecules at some of their relative orientations. Note, that in the case of N(A)H(A)...C(B) system the electrostatic interactions are quite weak. In such cases DFT (as also known from the literature) is not sufficient for the accurate determination of the molecular properties. We therefore decided to carry out the MP2 calculations, which are well suited for such problems. They are really time-consuming - the PQS quantum chemistry package does not allow the parallel MP2 calculations (this is actually the reason for the delay in answering the reports sent to us). MP2 results did not confirm the DFT predictions. The "MP2 dimer" we found turned out to be stabilized by two NH(A)...N(B) hydrogen bonds. Such bonds

enable the chemical exchange of protons between the heteroatoms rather than the proton transfer from N to C. We are inclined to trust the MP2 calculations in this particular case; the bimolecular mechanism seems to be the artifact of the DFT calculations. The relevant comments regarding the bimolecular mechanism are now in the revised manuscript. On the other hand, the remaining DFT results (i.e. these, regarding the unimolecular processes) are expected to be accurate. All processes investigated take place within the single, covalently bonded systems, for which the DFT calculations provide very accurate results.

Finally, we would like to emphasize that we are grateful to the reviewer for this comment, as well as for his/her effort to carry out the initial DFT calculations. The additional calculations we carried out were very educative to us.

We are very much grateful for the referee for its/their valuable suggestions. All of us (the authors) feel that the manuscript sounds much better now.

Instability of 2,2-di(pyridin-2-yl)acetic acid. Tautomerization versus decarboxylation

Received: 15.03.2010 / Accepted: 04.06.2010

Piotr Borowski^{1,✉}, Ryszard Gawinecki^{2,✉}, Anna Miłaczewska¹, Agnieszka Skotnicka², Krzysztof Woliński¹, and Agnieszka Brzyska¹

¹Department of Chemistry, Maria Curie-Skłodowska University, pl. Marii Curie Skłodowskiej 3, 20-031 Lublin, Poland

² Department of Chemistry, University of Technology and Life Sciences, Seminaryjna 3, PL-85-326, Bydgoszcz, Poland

✉Email: pibcio@vsop401.umcs.lublin.pl, gawiner@utp.edu.pl

Abstract

The DFT calculations at the B3LYP level with 6-311G** basis set were carried out in order to reveal whether tautomerization or decarboxylation is responsible for the instability of 2,2-di(pyridin-2-yl)acetic (DPA) and 1,8-diazafluorene-9-carboxylic (DAF) acids. The carboxyl protons in both compounds are involved in the intramolecular hydrogen bonds (the pyridine nitrogen atoms are the hydrogen bond acceptors). Although formation of two intramolecular OH...N hydrogen bonds in the enols of both carboxylic acids enables effective electron delocalization within the quasi rings (...HO-C=C-N), only ene-1,1-diol of DAF has somewhat lower energy than DAF itself (ΔE is *ca.* 7 kcal mol⁻¹). DPA and its enediol have comparable energies. Migration of the methine proton towards the carbonyl oxygen atom (to form enediols) requires overstepping the energy barriers of 55-57 kcal mol⁻¹ for both DPA and DAF. The enamionone tautomers of the acids, formed by migration of this proton towards the pyridine nitrogen atom, are thermodynamically somewhat more stable than the respective enediols. The energy barriers of these processes are equal to *ca.* 44 and 62 kcal mol⁻¹ for DPA and DAF, respectively. Thus, such tautomerization of the acids is not likely to proceed. On the other hand, the distinct energetic effects (*ca.* 15 kcal mol⁻¹) favor decarboxylation. This process involves formation of (*E*)-2-(pyridin-2(1*H*)-ylidenemethyl)pyridine and its cyclic

analogue followed by their tautomerization to (dipyridin-2-yl)methane and 1,8-diazafluorene, respectively. Although the later compound was found to be somewhat thermodynamically more stable, kinetic control of tautomerization of the former is more distinct.

Keywords Carboxylic acids · Decarboxylation · Tautomerization · Reaction path · Transition states · DFT calculations

Introduction

Ene-1,1-diols, often called enols of carboxylic acids, are intermediates in hydration of ketenes [1, 2]: $R_2C=C=O + H_2O \rightarrow R_2C=C(OH)_2 \rightarrow R_2CH-CO_2H$. These compounds are less stable than the corresponding carboxylic acids being energetically favored by delocalization of the lone electron pair of the hydroxy oxygen atom (Fig. 1) [1]. It is known, however, that ene-1,1-diols that contain bulky aromatic groups in the molecule, are more stable [1-4]. The hindered protonation of the β carbon atom in $Ar_2C^\beta=C(OH)_2$ caused by *ortho* alkyl groups (Ar = 2,4,6-trimethylphenyl, 2,4,6-triisopropylphenyl or 2,3,4,5,6-pentamethylphenyl) is responsible for such a behavior. Enediol of cyclopentadiene-1-carboxylic acid (Fig. 2) was found to be relatively stable [5]. Two intramolecular hydrogen bonds of the RAHB (Resonance-Assisted Hydrogen Bond) type [6-9] are expected to be present in its derivative annulated with two pyridine rings (Fig. 3). Unfortunately, neither 1,8-diazafluorene-9-carboxylic (9*H*-cyclopenta[1,2-*b*;3,4-*b'*]dipyridine-9-carboxylic) acid nor its enol are known, but close analogue of the former compound, 2,2-di(pyridin-2-yl)acetic acid, was claimed to be obtained earlier from 2-diazo-1,2-di(pyridin-2-yl)ethanone [10]. Since numerous heterocyclic acetic acids are potentially interesting as anti-arthritic agents [11, 12], the compounds mentioned above seem worthy to be studied from point of view of their stability.

<Figure 1>

<Figure 2>

<Figure 3>

Lossing of the CO₂ molecule by 2- and 4-pyridylacetic acids proceeds smoothly even below 100°C (this process is much more difficult for 3-pyridylacetic acid) [11-17]. 2-(Pyridin-2- and 4-yl)phenylacetic acids are also exceptionally unstable: benzylpyridines were found to be the only products of the acid hydrolysis of 2-(pyridin-2- and 4-yl)phenylacetone nitriles [18]. On the other hand, the enediol and enaminone tautomeric forms of the closely related 2,2-di(pyridin-2-yl)acetic acid (Fig. 4) can be stabilized by two intramolecular hydrogen bonds. Its tendency to decarboxylate is not reported in the only paper devoted to synthesis and properties of this compound [10].

<Figure 4>

Decarboxylation of carboxylic acid involves formation of carbon dioxide and an organic residue [16]. Organic product is usually stabilized by delocalization of its unshared electron pair. Formation of the intermediate zwitterion $\text{HOCO-C}_5\text{H}_4\text{N} \rightarrow {}^{\ominus}\text{OCO-C}_5\text{H}_4\text{N}^{\oplus}\text{H}$ is a common step in the mechanism of enzyme-catalyzed decarboxylations of 2- and 4-pyridylacetic acids [12, 14, 17]. Electron delocalization is particularly important in enzymatic reactions, where an “electron sink” is generally provided by a coenzyme [16].

Despite their instability, the labile compounds may appear as intermediates in numerous (bio)chemical processes. Explanation what are the products these derivatives are transformed to, seems very important. Numerous attempts done in our laboratory to obtain 2,2-di(pyridin-2-yl)acetic acid (**1a**, Fig. 5) from 2-diazo-1,2-di(pyridin-2-yl)ethanone according to the known procedure [10] as well as by hydrolysis of 2,2-di(pyridin-2-yl)acetonitrile (the standard procedure) were unsuccessful. Irrespective of the reason of inaccessibility of this compound to us, its properties can still be discovered by quantum chemical calculations. In the present paper 2,2-di(pyridin-2-yl)acetic (**1a**) and 1,8-diazafluorene-9-carboxylic (**1b**) acids are considered to be susceptible to tautomerization and decarboxylation. The related pyridylacetic acids were earlier used as the models when studying decarboxylation mechanism of aminoacids [19]. It is noteworthy that numerous heterocyclic derivatives of acetic acid are potentially interesting as anti-arthritis agents [20].

Computational details

Density functional theory (DFT, see *e.g.* [21]) has been recognized for years to be capable of predicting the very accurate conformations of the covalently bonded systems. Thus, its use in the present paper is justifiable. All calculations were carried out using B3LYP hybrid functional [22, 23] with the 6-311G** basis set [24].

Formulas of 2,2-di(pyridin-2-yl)acetic (**1a**) and 1,8-diazafluorene-9-carboxylic (**1b**) acids, their enol (**2a,b**) and enaminone (**3a,b**) tautomeric forms as well as the (expected) intermediates (**4a,b**) and final products of the decarboxylation process (**5a,b**) are depicted in Fig. 5, which also shows numbering of heavy atoms. It should be noted that the carboxyl hydrogen atom H9 (in **1**, **2** and **3**) has the same number even if it is bound to N1 (in **4**) or C7 (in **5**). Formulas of the transition states that are (or may be) formed during decarboxylation of **1a** and **1b** can be seen in Fig. 6. The geometry optimization of all substrates, products and

transition states was carried out first. Then, the harmonic frequencies were calculated to establish the types of stationary points, and to find the zero-point energy (ZPE) corrections for the energy barriers and the energetic effects of the processes investigated in the present work. All frequencies for systems **1–5(a,b)** were real. On the other hand, one imaginary frequency was found for transition states **TS(1-4)a,b**. Analysis of the eigenvectors corresponding to the imaginary frequencies provided us with the information about the possible products "on each side" of a transition state at a given stage of the reaction.

<Figure 5>

<Figure 6>

Geometry optimization for the transition state is much more complex than for the stable system. This prompted us to carry out some initial, point-wise calculations, corresponding to the so-called distinguished reaction coordinate (DRC). This procedure is not recommended for the accurate description of the reaction path, for example on account of possible discontinuities of energy (and geometrical parameters) as a function of DRC (*i.e.* some selected geometrical parameter, *e.g.* bond length). It may, however, provide a reasonable initial structure for which typical algorithms are capable of converging quickly to the required transition state. Therefore, the C7C8 bond was selected as the DRC in reactions **1** \rightarrow **4** + CO₂. Its length, R , was gradually increased from the equilibrium value found for **1** (the applied increment was 0.1Å), the remaining parameters were optimized, and the geometry corresponding to the highest energy was determined. Since H9 turned out to be still bound to the carboxylic oxygen atom, it was placed in the middle of the O9...N1 distance prior to running the transition state search. On the other hand, the two internal coordinates $r_1 = \text{H9N1}$ and $r_2 = \text{H9C7}$ (*cf.* Fig. 5) were selected for the description of the proton migration in the **4** \rightarrow **5** tautomerization. Energies of structures optimized for the remaining geometrical parameters were then computed at a grid of selected linearly independent points. Then, the cross-section of PES (see Fig. 7 for an example), approximated by the 3rd degree polynomial, was subjected to straightforward search of the saddle point. All initial structures obtained in this way turned out to converge quickly to the corresponding transition states by following (maximizing along) the lowest (negative) Hessian eigenmode. In order to follow the reaction paths, concept of the so-called intrinsic reaction coordinate (IRC) [25] in mass-weighted Cartesian coordinates was used. All calculations were carried out with the parallel version of the PQS quantum chemistry package [26, 27].

<Figure 7>

Results and discussion

Molecular geometries

The optimized structures of carboxylic acids as well as these of the enol and enaminone tautomeric forms and products of their decarboxylation (dipyridyl-2-ylmethane and its 1,2-dihydro tautomeric form) are depicted in Fig. 8. Their most important geometrical parameters, as well as geometrical parameters of the transition states **TS(1-4)a,b** are presented in Tables 1 and 2.

<Figure 8>

<Table 1>

< Table 2>

The most significant conclusions regarding the molecular geometries are as follow:

1. Arrangement of the N1 and N1' atoms in the most stable conformer of 2,2-di(pyridin-2-yl)acetic acid **1a** is *trans*-like relative to the C2C7C2' link (Fig. 8). Turning of one pyridine ring in **1a** by *ca.* 90° around the C7C2' bond increases the energy by only 0.3 kcal mol⁻¹. Linking of the pyridine rings *via* the C3C3' bond in **1b** prevents their free rotation and makes the molecule rigid. Note that the N1C2C7C2' and N1'C2'C7C2 torsion angles in **1b** are close to 180°, *i.e.* the pyridine rings in the molecule are nearly coplanar. The hydroxyl groups both in **1a** and **1b** are involved in the intramolecular hydrogen bond with the N1 atom being the hydrogen bond acceptor. The OH bond in **1a** is somewhat longer than 0.99 Å (a typical OH bond length in the dimers of ordinary carboxylic acids where very strong intermolecular hydrogen bonds are present). On the other hand, the OH bond in **1b** is shorter (*ca.* 0.98 Å). Rigidity of the **1b** molecule and, consequently, steeper energy increase along the interring torsional motions, prevent the H9 and N1 atoms to approach each other as close as in **1a**. This results in elongation (weakening) of the H...N1 hydrogen bond (1.918 Å in **1b** vs. 1.738 Å in **1a**) and shortening (strengthening) of the O9H bond. The carbon-nitrogen bond lengths in the pyridine rings of **1a** and **1b** are close

to these in pyridine itself (1.337 Å; geometry optimized at the B3LYP/6-311G** level). The same applies to the ring carbon-carbon bond lengths which are comparable to the average bond length in pyridine (1.393 Å). Slight elongation of the carbon-nitrogen bonds in **1a** and **1b** is observed for the ring involved in the hydrogen bonding. The valence CNC angles in these systems are also comparable to those found in the molecule of pyridine (117.2°).

2. Formation of the H···N1 and H···N1' hydrogen bonds in **2a** and **2b** affects the hybridization of C7 and shortens the C7C8 bond lengths (1.419 Å in **2a** and 1.376 Å in **2b**) as compared to these in **1a** and **1b**. These bonds resemble more the carbon-carbon bonds in the benzene ring (~1.39 Å) rather than those in alkenes (~1.33 Å). It should be noted that C7C8 bond in **2a** is longer, while this in **2b** is shorter than 1.39 Å. Effective electron delocalization in the quasi rings that involve OH···N fragments results also in shortening of the C7C2 and C7C2' bonds both in **2a** and **2b** (they are still significantly longer than the aromatic carbon-carbon bonds) as compared to these in **1a** and **1b** (the C7C8, C7C2 and C7C2' bonds in their molecules are typical carbon-carbon single bonds). The H9O9 and the hydrogen H···N1⁽ⁱ⁾ bond lengths in **2a,b** follow the same pattern as these in the molecules of **1a,b**. Moreover, C3C3' bond in **2b** is much longer than C7C2⁽ⁱ⁾ and C2⁽ⁱ⁾C3⁽ⁱ⁾ bonds (which have comparable lengths, *cf.* Table 1). Thus, aromaticity of the five membered ring in **2b** is doubtful what negates stabilization of this form by resonance suggested in Fig. 3.
3. The NH···O hydrogen bonds are present in the enaminone tautomeric forms **3a** and **3b** (these bonds are longer than the OH···N hydrogen bonds in **2a** and **2b**). Contribution of the zwitterionic structures of **3** (*cf.* Fig. 5) is manifested in shortening of the C7C8 bonds (this effect is not as significant as for **2**) and elongation of the C8O10 bonds as compared to **1**.
4. **4a** and **4b** seem likely to be the intermediate products of decarboxylation of **1a** and **1b**, respectively. Both these molecules are planar. Hydrogen atom involved in the H···N1 hydrogen bonding in **1a** and **1b** is bound to N1. The N1H bond lengths (1.009 Å in both systems) are in between these found for pyrrole (1.006 Å) and aliphatic amines (1.015 Å; geometry optimized at the B3LYP/6-311G** level). The C7C2 and C7C2' bond lengths are intermediate between these of the single and double carbon-carbon bonds. In both **4a** and **4b** the C7C2 bonds are shorter, while C7C2' are longer than 1.39 Å (Table 1).

5. **5a** and **5b** are probably the final products of decarboxylation of **1a** and **1b**. Their geometrical parameters remain similar to these found for **1a** and **1b**, as well as those in pyridine itself. Note that the pyridine rings in **5b** are coplanar.

Reaction paths and energetic effects

Calculations of the energetic effects of the most intuitive reactions **1** \rightarrow **5** + CO₂ reveal that products are by *ca.* 13.6 (case **a**) and *ca.* 15.8 kcal mol⁻¹ (case **b**) more stable than substrates. All energetic effects $|E_{\text{products}} - E_{\text{substrates}}|$ and energy barriers $E_{\text{TS}} - E_{\text{substrates/products}}$ discussed (denoted as ΔE) were corrected for the zero-point energy, ZPE. They are depicted in Fig. 9. The data used in order to obtain these values (*i.e.* total energies of the molecules and ZPE corrections of all stable structures and transition states) are reported in Table 3. Note that for the brevity reason the ΔG values were calculated for decarboxylation processes only. Comparable entropies of the substrates and products for the tautomerization processes suggest that the ΔE and ΔG values also approximate each other.

<Figure 9>

<Table 3>

Ene-1,1-diols **2** have lower energies than the respective acids **1**: the energy lowering is equal to approximately 0.7 and 7 kcal mol⁻¹ for **2a** and **2b**, respectively (Fig. 9). The energy barriers for the proton migration from C7 towards the carbonyl oxygen atom O10 (this processes proceed *via* **TS1** transition states) are nearly the same for **a** and **b** and amount to *ca.* 55 kcal mol⁻¹. The enaminone tautomeric forms **3a,b** are thermodynamically somewhat more stable than **2a,b** (by nearly 4 kcal mol⁻¹ in the case of **3b**). However, the energy barriers for the migration of proton H7 towards N1', associated with the presence of **TS2a** and **TS2b** transition states, differ significantly: the calculated ΔE values are equal to *ca.* 44 and *ca.* 62 kcal mol⁻¹ for **1a** \rightarrow **3a** and **1b** \rightarrow **3b**, respectively. In a view of finding more energetically favorable processes from the thermodynamic and kinetic point of view (*vide infra*) we conclude that tautomerization of **1a** and **1b** is not likely to proceed. Among all investigated processes, namely **1** \rightarrow **2**, **1** \rightarrow **3**, and **1** \rightarrow **5** + CO₂, the most distinct energetic effect can be seen for **1** \rightarrow **5** + CO₂ (for both **a** and **b**, *cf.* Fig. 9). These processes will be discussed in details.

Rupture of the C7C8 bond in the $\mathbf{1} \rightarrow \mathbf{4} + \text{CO}_2$ reaction is probably followed by migration of the carboxylic hydrogen atom to C7 (this results in formation of $\mathbf{5}$). The concerted and step-wise mechanisms have to be considered here. In the first one, the eigenmode (atomic displacements) corresponding to the imaginary frequency should correspond to simultaneous detachment of CO_2 and migration of the carboxylic proton H9 towards C7. The later mechanism is expected to involve a few different transition states. The case **a** will be considered first. A quick glance at the structure of **1a** points at the second, *i.e.* step-wise mechanism. The reason for this is a significant energy increase when H9 approaches C7, while C7 is still bound to C8. It is shown in Fig. 10 as a steep, violet (turning to blue at larger values of R) “slope” on a cross-section of the potential energy hypersurface of **1a**. In addition, elongation of the C7C8 bond reveals that there is a clear trend for the H9 atom to approach N1, *i.e.* to form **4a**. Therefore one should search for a transition state that appears in the course of reaction $\mathbf{1a} \rightarrow \mathbf{TS3a} \rightarrow \mathbf{4a} + \text{CO}_2$. It was found to be nearly 20 kcal mol^{-1} above **1a**. The calculated ΔG value corresponding to the reported ΔE amounts to $18.33 \text{ kcal mol}^{-1}$. This value is known to be low enough for the process that is fast under standard conditions. Analysis of geometrical parameters shows that C7C8 bond in **TS3a** is significantly longer than that in **1a**, and that the H \cdots N1 bond remains close to that of **4a** (*cf.* Tables 1 and 2). The structure of **TS3a** is depicted in Fig. 11 (the eigenmode, corresponding to the imaginary frequency equal to $i320\text{cm}^{-1}$, is also shown there). Following the reaction path from **TS3a** along the intrinsic reaction coordinate (IRC), **1a** or **4a** + CO_2 were obtained. No energy lowering is observed at this stage of decarboxylation. However, value of the Gibbs free energy of the products calculated at 298 K is by more than 12 kcal mol^{-1} lower than that of **1a**. Although rotational and vibrational entropies were also changed ($\Delta S_{\text{rot}} = 11.9 \text{ cal mol}^{-1} \text{ K}^{-1}$ and $\Delta S_{\text{vib}} = -12.2 \text{ cal mol}^{-1} \text{ K}^{-1}$), significant increase in the translational entropy ($\Delta S_{\text{trans}} = 36.6 \text{ cal mol}^{-1} \text{ K}^{-1}$) gives the major contribution to the reported value of ΔG . The low energy barrier being $< 20 \text{ kcal mol}^{-1}$ (corresponding to energy of quanta in the near IR region) as well as negative value of ΔG clearly show that **1a** decomposes spontaneously (and rapidly) to form **4a** and CO_2 . This proves that Eistert and Schade [10] could not obtain **1a**. It is probably why we were not able to obtain this compound starting from 2-diazo-1,2-di(pyridin-2-yl)ethanone [10] as well as by hydrolysis of 2,2-di(pyridin-2-yl)acetonitrile (the standard procedure).

<Figure 10>

<Figure 11>

4a is probably an intermediate in the process of decarboxylation of **1a**. In order to obtain **5a**, which is the most stable system studied (at least at the B3LYP level, *cf.* Fig. 9 and Table 3), the C7H9 bond has to be formed and, at the same time, the N1H9 bond has to be broken. It was not clear to us what is the mechanism of this step (*i.e.* unimolecular or bimolecular). It was initially assumed that the rearrangement takes place within the single molecule. This process is accompanied by breaking of the planar symmetry of **4a** (note that C7 atom has to change its hybridization from sp^2 in **4a** to sp^3 in **5a**). The search for another transition state (**TS4a**) was carried out in the way described in Section 2. Its structure along with the imaginary eigenmode ($i1834\text{cm}^{-1}$) is shown in Fig. 11. Location of H9 more or less half way between N1 and C7 (*cf.* Table 2) is the characteristic feature of this transition state. The energy barrier $\Delta E = 42.37 \text{ kcal mol}^{-1}$ that has to be overstepped, corresponds to ΔG value of *ca.* 38 kcal mol^{-1} . It is two times higher than that for the CO_2 detachment. This seems to be mostly due to the high strain within the 4-membered ring formed in the **TS4a** transition state. Thus, this step of the decarboxylation process, though spontaneous from the thermodynamic point of view, is expected to be much slower than the former one.

An alternative mechanism involves two molecules of **4a**. The B3LYP calculations show, that they are capable of forming a relatively stable dimer possessing the C_2 symmetry. It is depicted on Fig. 12a; the binding energy, counterpoise (CP) corrected for the basis set superposition error [28] and ZPE corrected, is equal to $4.26 \text{ kcal mol}^{-1}$. The transition state, corresponding to the imaginary frequency of $i1281 \text{ cm}^{-1}$, was found to be only $14.58 \text{ kcal mol}^{-1}$ above the dimer (the ZPE corrected value; the corresponding ΔG value is $11.41 \text{ kcal mol}^{-1}$). Analysis of the imaginary eigenmode shows that this is the transition state for the migration of the H9 atom from N1 atom of one **4a** molecule to the C7 atom of the other **4a** molecule (actually, two molecules of **5a** were finally obtained by following the reaction path along the intrinsic reaction coordinate). The B3LYP energetic effect of the overall reaction, *i.e.* $(\mathbf{4a})_2 \rightarrow 2 \mathbf{5a}$, is $10.85 \text{ kcal mol}^{-1}$ per molecule ($\Delta G=17.14 \text{ kcal mol}^{-1}$). However, it should be noted that the dimer predicted by B3LYP calculations is stabilized by the interactions of the NH fragment of one molecule (a rather weak dipole) with the non-polar $\text{C}\equiv\text{C}\equiv\text{C}$ system of the other molecule (the quadrupole, *cf.* Fig. 12a). Thus, the dispersive-type interactions that show the $U_{\text{disp}} \sim r^{-6}$ dependence on distance, are not negligible as compared to the weak electrostatic dipole-quadrupole interactions $U_{\text{dip-quad}} \sim r^{-4}$. The same type of interactions are expected in the transition state. Since DFT is known to poorly describe the dispersive interactions, we decided to investigate this problem using the MP2 method with the same basis set. The

geometry optimization of the dimer of **4a** was carried out at the MP2/6-311G** level, using the B3LYP structure as an initial guess. This time we did not obtain the analogous dimer; two NH...N hydrogen bonds were formed instead. This complex, for which the CP corrected binding energy is 14.29 kcal mol⁻¹ (the MP2 frequencies were not calculated for practical reasons, but the ZPE estimate obtained at the DFT level, would further reduce this value by *ca.* 0.7 kcal mol⁻¹), is shown in Fig. 12b. Thus it seems, that the DFT calculations overestimate the dispersive interactions when two molecules of **4a** approach each other.

<Figure 12>

In a view of the MP2 results we conclude that the unimolecular mechanism is responsible for the formation of **5a**. Note that the NH...N links are typically responsible for the chemical exchange of the labile protons. Actually, compounds **4a** and **5a** were obtained by following the reaction path from **TS4a** along the intrinsic reaction coordinate. It should be noted that the reported energy barrier of *ca.* 40 kcal mol⁻¹ is comparable to that found for the **1a** → **TS2a** → **3a** reaction. However, low energy barrier of the CO₂ detachment, and significantly higher stability of **5a** as compared to **3a**, proves that synthesis of **1a** [10] could not be successful: this compound spontaneously decarboxylates when it is formed.

Structures of the **TS3b** and **TS4b** transition states in decarboxylation of **1b** as well as imaginary eigenmodes (corresponding to frequencies equal to *i*332cm⁻¹ and *i*2050cm⁻¹, respectively) are depicted in Fig. 13. Weaker intramolecular hydrogen bond in **1b** as compared to that in **1a** (*cf.* Table 1), is to some extent responsible for the lower energy barrier ($\Delta G \approx 13$ kcal mol⁻¹, *cf.* Fig. 9) of the dissociation process **1b** → **4b** + CO₂, and for the formation of the NIH bond in **4b**. This stage of the reaction is expected to be spontaneous as well: energy lowering ($\Delta E = 4.8$ kcal mol⁻¹, and $\Delta G = 17.24$ kcal mol⁻¹) was observed. The most significant difference between this (**b**) and previous (**a**) decarboxylation processes is an increase of the energy barrier associated with the migration of H9 towards C7 in the **4b** → **5b** tautomerization by more than 20 kcal mol⁻¹. This value refers to both ΔE and ΔG . Note, that we assume the unimolecular mechanism of tautomerization, in spite of finding a relatively stable dimer of **4b** at the B3LYP level, analogous to the dimer of **4a**, for which the CP corrected binding energy is equal to *ca.* 6 kcal mol⁻¹ (the imaginary eigenmode for the transition state found for (**4b**)₂ → 2 **5b** reaction corresponds to *i*1149cm⁻¹, the $\Delta E/\Delta G$ energy barriers are *ca.* 14.7/12.6 kcal mol⁻¹, and the $\Delta E/\Delta G$ energetic effects are *ca.* 7.5/13.6 kcal mol⁻¹ per molecule, respectively). However, this time the lengthy MP2 calculations were not

carried out. The reason for this can be easily understood when structures involved in the described processes are analyzed. The change in the hybridization of C7 to sp^3 when going from **4b** to **5b** via **TS4b** is associated with breaking of the planar symmetry of **4b**. Similar behavior is also observed in reaction **4a** \rightarrow **5a**. One should keep in mind, however, that the C3C3' bond makes the molecules **4b** and **5b** rigid (*cf.* Section 3.1), and this results in a steeper energy increase under torsional distortions. As a consequence, significantly risen energy barrier of the **4b** \rightarrow **5b** step (*ca.* 60 kcal mol⁻¹) may preclude tautomerization to proceed. Thus, **4b** may appear to be the final product of decarboxylation of **1b**. In addition, it can be seen from Fig. 9 and Table 3 that although **5b** is thermodynamically more stable than **5a**, kinetic control of the **4a** \rightarrow **5a** process is more distinct than that of **4b** \rightarrow **5b**.

<Figure 13>

Finally we would like to point out that the bimolecular mechanism was also considered in the case of the enolization process of **1a**. The stable dimer, that could initiate the H proton transfer from C7 atom of one molecule of **1a** to O10 atom of the other molecule of **1a**, was found at the B3LYP level. It is shown in Fig. 14. This time no transition state associated with such a migration was found (the MP2 calculations were not carried out).

<Figure 14>

Conclusions

Tautomerization and decarboxylation of 2,2-di(pyridin-2-yl)acetic acid were considered to be responsible for its instability. DFT/B3LYP/6-311G** calculations show that the products of decarboxylation of this acid and its rigid cyclic analogue, 1,8-diazafluorene-9-carboxylic acid, are more energetically favorable than the corresponding ene-1,1-diols (products of migration of the methine proton towards the carbonyl oxygen atom) and enaminones (products of migration of the same proton towards the pyridine nitrogen atom). The later tautomers were found to be thermodynamically more stable than enediols. Aromatization of the five membered ring has no effect on stabilization of ene-1,1-diol of 1,8-diazafluorene-9-carboxylic acid. Detachment of CO₂ from 2,2-di(pyridin-2-yl)acetic and 1,8-diazafluorene-9-carboxylic acids to give (*E*)-2-(pyridin-2(1*H*)-ylidenemethyl)pyridine and its cyclic analogue, respectively, may be followed by tautomerization of these by-products into (dipyridin-2-

yl)methane and 1,8-diazafluorene. The calculated energy barriers for the CO₂ detachment correspond to quanta of IR radiation, so they can be easily overstepped in the course of reactions expected to afford 2,2-di(pyridin-2-yl)acetic and 1,8-diazafluorene-9-carboxylic acids. Thus, spontaneous decarboxylation of the former is in line with the unsuccessful synthetic efforts.

Despite their instability, the labile compounds may appear as the intermediates in numerous (bio)chemical processes. Conclusions of the present paper may be valid also for other substituted acetic acids (and their homologues) that carry electronegative heteroatoms in the *gamma* positions, such as diacylacetic acids and their derivatives (to be also known as unstable compounds).

References

1. Frey J, Rappoport Z (1996) *J Am Chem Soc* 118:5169-5181
2. Allen BM, Hegarty AF, O'Neill P, Nguyen MT (1992) *J Chem Soc Perkin Trans 2*:927-934
3. O'Neill P, Hegarty AF (1987) *J Chem Soc Chem Commun* 744-745
4. Allen BM, Hegarty AF, O'Neill P (1997) *J Chem Soc Perkin Trans 2*:2733-2736
5. Urwyler B, Wirz J (1990) *Angew Chem Int Ed Engl* 29:790-792
6. Gilli G, Belluci F, Ferretti V, Bertolasi V (1989) *J Am Chem Soc* 111:1023-1028
7. Bertolasi V, Gilli P, Ferretti V, Gilli G (1991) *J Am Chem Soc* 113:4917-4925
8. Gilli P, Bertolasi V, Ferretti V, Gilli G (1994) *J Am Chem Soc* 116:909-915
9. Bertolasi V, Gilli P, Ferretti V, Gilli G (1996) *Chem Eur J* 2:925-934
10. Eistert B, Schade W (1958) *Chem Ber* 91:1411-1415
11. Taylor PJ (1972) *J Chem Soc Perkin Trans 2*:1077-1086
12. Sicinska D, Lewandowicz A, Vokal B, Paneth P (2001) *J Org Chem* 66:5534-5536
13. Katritzky AR, Pozharsky AF (2000) *Handbook of Heterocyclic Chemistry*, 2nd edn. Pergamon, Elsevier, Amsterdam
14. Doering W von E, Pasternak VZ (1950) *J Am Chem Soc* 72:143-147
15. Sicinska D, Truhlar DG, Paneth P (2001) *J Am Chem Soc* 123:7683-7686
16. Headley GW, O'Leary MH (1990) *J Am Chem Soc* 112:1894-1896
17. Marlier JF, O'Leary MH (1986) *J Am Chem Soc* 108:4896-4899
18. Panizzon L (1944) *Helv Chim Acta* 27:1748-1756
19. O'Leary MH (1988) *Acc Chem Res* 21:450-455 and papers cited therein
20. British Patents 1,099,389; 1,121,922; 1,139,940; 1,147,068 and 1,164,510.
21. Parr RG, Yang W (1989) *Density-Functional Theory of Atoms and Molecules*. Oxford University Press, New York
22. Becke AD (1993) *J Chem Phys* 98:5648-5652
23. Lee C, Yang W, Parr RG (1993) *Phys Rev B* 37:785-769
24. Krishnan R, Binkley JS, Seeger R, Pople JA (1980) *J Chem Phys* 72:650-654
25. Fukui K (1970) *J Phys Chem* 74:4161-4163
26. Baker J, Wolinski K, Malagoli M, Kinghorn D, Wolinski P, Magyarfalvi G, Saebo S, Janowski T, Pulay P (2009) *J Comput Chem* 30(2):317-335
27. PQS version 3.3, Parallel Quantum Solutions; 2013 Green Acres Road, Fayetteville, Arkansas 72703, USA

28. Boys SF, Bernardi F (1970) *Mol Phys* 19:553-566

Tables

Table 1 Selected optimized (B3LYP/6-311G**) bond lengths [\AA] as well as valence and torsion angles [deg] in compounds **1-5**

Bond/angle	1a	1b	2a	2b	3a	3b	4a	4b	5a	5b
O9H9	0.993	0.981	1.021	0.990	1.000	0.981	–	–	–	–
N1H9	1.738	1.918	1.572	1.965	1.654	2.005	1.009	1.009	–	–
O10H7	–	–	1.021	0.990	1.606	2.138	–	–	–	–
N1'H7	–	–	1.572	1.965	1.047	1.021	–	–	–	–
C8O10	1.201	1.195	1.306	1.315	1.238	1.223	–	–	–	–
C8O9	1.339	1.345	1.306	1.315	1.328	1.344	–	–	–	–
C7H7	1.089	1.098	–	–	–	–	1.087	1.079	1.091	1.095
C7H9	–	–	–	–	–	–	–	–	1.091	1.095
C7C2	1.523	1.513	1.462	1.433	1.467	1.436	1.375	1.372	1.517	1.511
C7C2'	1.534	1.514	1.462	1.433	1.415	1.387	1.444	1.441	1.517	1.511
C7C8	1.546	1.550	1.419	1.376	1.479	1.450	–	–	–	–
N1C2	1.340	1.325	1.359	1.338	1.356	1.341	1.402	1.377	1.340	1.326
N1C6	1.338	1.344	1.336	1.340	1.335	1.336	1.365	1.363	1.337	1.342
N1'C2'	1.338	1.323	1.359	1.338	1.380	1.359	1.355	1.343	1.340	1.326
N1'C6'	1.335	1.341	1.336	1.340	1.350	1.356	1.333	1.334	1.337	1.342
C2C3	1.397	1.407	1.415	1.428	1.414	1.433	1.445	1.469	1.399	1.412
C3C4	1.389	1.391	1.383	1.389	1.384	1.389	1.360	1.367	1.390	1.391
C4C5	1.394	1.396	1.398	1.398	1.396	1.395	1.432	1.423	1.392	1.394
C5C6	1.388	1.393	1.384	1.397	1.387	1.400	1.357	1.368	1.392	1.395
C2'C3'	1.397	1.412	1.415	1.428	1.433	1.449	1.417	1.435	1.399	1.412
C3'C4'	1.391	1.391	1.383	1.389	1.369	1.375	1.382	1.390	1.390	1.391
C4'C5'	1.391	1.393	1.398	1.398	1.417	1.417	1.397	1.391	1.392	1.394
C5'C6'	1.392	1.396	1.384	1.397	1.366	1.375	1.390	1.403	1.392	1.395
C3C3'	–	1.463	–	1.461	–	1.451	–	1.442	–	1.463
C2C7C2'	109.0	101.8	122.8	106.9	121.7	105.9	129.1	106.5	112.1	102.4
C2N1C6	119.3	116.7	120.9	115.8	120.5	116.1	124.9	122.3	118.1	116.2
C2'N1'C6'	118.2	116.1	120.9	115.8	124.9	121.4	118.7	116.0	118.1	116.2
C2C7C8	116.6	113.3	118.6	126.5	120.2	129.8	–	–	–	–
C2'C7C8	111.1	116.9	118.6	126.5	118.1	124.3	–	–	–	–
N1C2C7C8	37.0	-52.0	19.8	0.0	28.0	0.0	–	–	–	–
N1'C2'C7C8	145.2	58.8	19.8	0.0	12.2	0.0	–	–	–	–
N1C2C7C2'	-89.8	178.3	-160.2	180.0	-152.1	180.0	180.0	180.0	-95.8	180.0
N1'C2'C7C2'	-85.0	-177.3	-160.2	180.0	-167.7	180.0	0.0	180.0	-95.8	180.0

Table 2 Selected optimized (B3LYP/6-311G**) bond lengths [\AA] as well as valence and torsion angles [deg] in the transition states

Bond/angle	TS1a	TS1b	TS2a	TS2b	TS3a	TS3b	TS4a	TS4b
O9H9	1.009	0.984	0.994	0.982	1.829	1.549	–	–
N1H9	1.754	2.078	1.721	1.883	1.030	1.093	1.263	1.356
O10H7	1.246	1.345	2.881	2.861	–	–	–	–
N1'H7	2.829	2.596	1.271	1.358	–	–	–	–
C8O10	1.265	1.260	1.216	1.208	1.192	1.204	–	–
C8O9	1.290	1.307	1.338	1.350	1.221	1.262	–	–
C7H7	1.526	1.455	1.583	2.115	1.085	1.093	1.091	1.086
C7H9	2.459	2.464	1.362	2.355	–	–	1.608	1.609
C7C2	1.485	1.456	1.463	1.417	1.432	1.464	1.467	1.435
C7C2'	1.493	1.488	1.490	1.434	1.492	1.499	1.455	1.460
C7C8	1.489	1.452	1.495	1.475	1.951	1.692	–	–
N1C2	1.354	1.336	1.354	1.357	1.371	1.335	1.359	1.343
N1C6	1.337	1.342	1.335	1.322	1.356	1.351	1.343	1.338
N1'C2'	1.345	1.328	1.351	1.427	1.345	1.327	1.353	1.341
N1'C6'	1.335	1.338	1.341	1.344	1.333	1.339	1.335	1.331
C2C3	1.403	1.418	1.413	1.437	1.416	1.411	1.399	1.411
C3C4	1.387	1.391	1.384	1.403	1.374	1.388	1.387	1.399
C4C5	1.395	1.396	1.397	1.381	1.414	1.406	1.405	1.401
C5C6	1.388	1.396	1.387	1.415	1.367	1.383	1.384	1.403
C2'C3'	1.407	1.427	1.390	1.483	1.405	1.422	1.413	1.444
C3'C4'	1.386	1.391	1.392	1.382	1.388	1.391	1.383	1.394
C4'C5'	1.395	1.392	1.399	1.400	1.392	1.392	1.398	1.388
C5'C6'	1.390	1.398	1.386	1.394	1.392	1.398	1.390	1.404
C3C3'	–	1.455	–	1.420	–	1.460	–	1.452
C2C7C2'	117.8	104.6	119.9	105.4	122.7	101.4	121.3	102.0
C2N1C6	119.7	116.0	119.9	116.7	124.1	120.8	123.3	118.4
C2'N1'C6'	118.9	116.2	123.1	115.6	118.8	116.2	118.5	116.5
C2C7C8	113.7	121.0	123.1	127.0	104.2	107.7	–	–
C2'C7C8	112.3	127.7	111.0	127.2	101.7	122.7	–	–
N1C2C7C8	-30.2	10.3	23.2	-5.2	54.7	-41.3	–	–
N1'C2'C7C8	-1.7	-22.8	-95.8	13.2	104.5	62.8	–	–
N1C2C7C2'	104.3	163.7	173.6	-178.8	-59.6	-171.3	138.3	-157.3
N1'C2'C7C2'	-136.7	-173.7	110.5	-173.2	-139.9	-177.4	-12.6	-176.9

Table 3 Total energies (in a.u.) and ZPE corrections (in kcal mol⁻¹) of the substrates, products and transition states

	E	ZPE
2a	-723.447573	125.63
3a	-723.449268	126.14
↑		
TS1a	-723.350792	122.21
TS2a	-723.370685	122.49
↓		
1a	-723.447339	126.17
↓		
TS3a	-723.413217	124.57
↓		
4a + CO₂	-723.443569	123.81
↓		
TS4a + CO₂	-723.369568	119.72
↓		
5a + CO₂	-723.465199	123.80
2b	-722.252866	113.08
3b	-722.259203	113.25
↑		
TS1b	-722.146161	108.67
TS2b	-722.135826	108.65
↓		
1b	-722.240663	112.39
↓		
TS3b	-722.213498	110.27
↓		
4b + CO₂	-722.245186	110.43
↓		
TS4b + CO₂	-722.136557	105.69
↓		
5b + CO₂	-722.262235	110.10

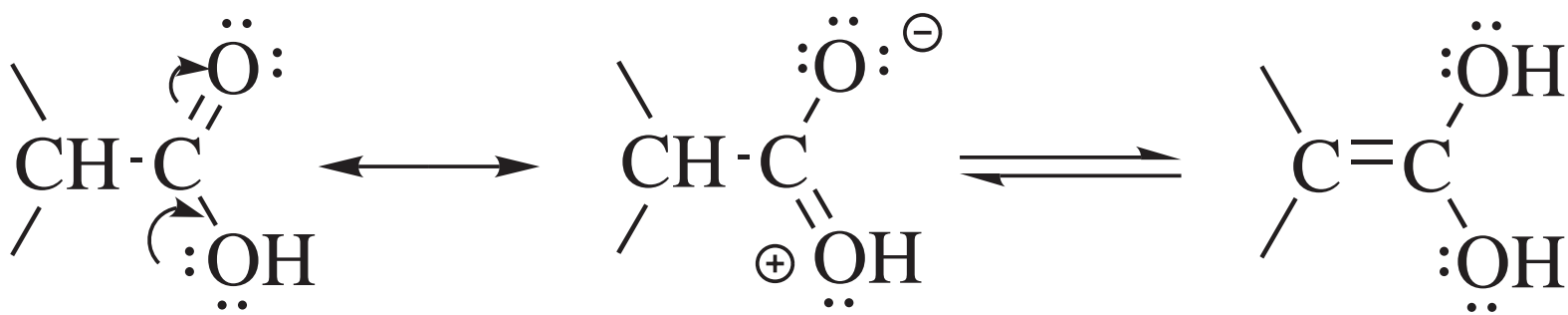
Figure captions

- Fig. 1** Relation between carboxylic acids and ene-1,1-diols
- Fig. 2** Cyclopentadiene-1-carboxylic acid and its enol
- Fig. 3** Relation between 1,8-diazafluorene-9-carboxylic acid and its enol
- Fig. 4** Relation between 2,2-di(pyridin-2-yl)acetic (R = H) and 1,8-diazafluorene-9-carboxylic (R = none) acids and its tautomers
- Fig. 5** Formulas of the compounds studied and the numbering of the heavy atoms
- Fig. 6** Formulas of the transition states studied in this work
- Fig. 7** The cross-section of the potential energy surface (PES) corresponding to the proton migration in **4a** → **5a** reaction (see text for the definition of the internal coordinates)
- Fig. 8** Optimized structures of the substrates and products of the tautomerization/decarboxylation processes
- Fig. 9** Reaction paths, ZPE corrected energy barriers and energetic effects (ΔE in kcal mol⁻¹) in tautomerization and decarboxylation of **1a** and **1b**. The calculated ΔG values (for decarboxylation processes only) are reported in parentheses
- Fig. 10** Cross-section of the potential energy surface (PES) of **1a** corresponding to the rupture of C7C8 (variable R) bond and simultaneous migration of the hydroxyl proton towards C7 (variable r_2)
- Fig. 11** Transition states **TS3a** and **TS4a**. The arrows show the atomic displacement corresponding to the imaginary frequencies
- Fig. 12** The dimers of **4a** predicted at (a) B3LYP and (b) MP2 levels

Fig. 13 Transition states **TS3b** and **TS4b**. The arrows show the atomic displacement corresponding to the imaginary frequencies

Fig. 14 The dimer of **1a** predicted at B3LYP level

Figure 1
[Click here to download line figure: Fig. 1 eps.eps](#)



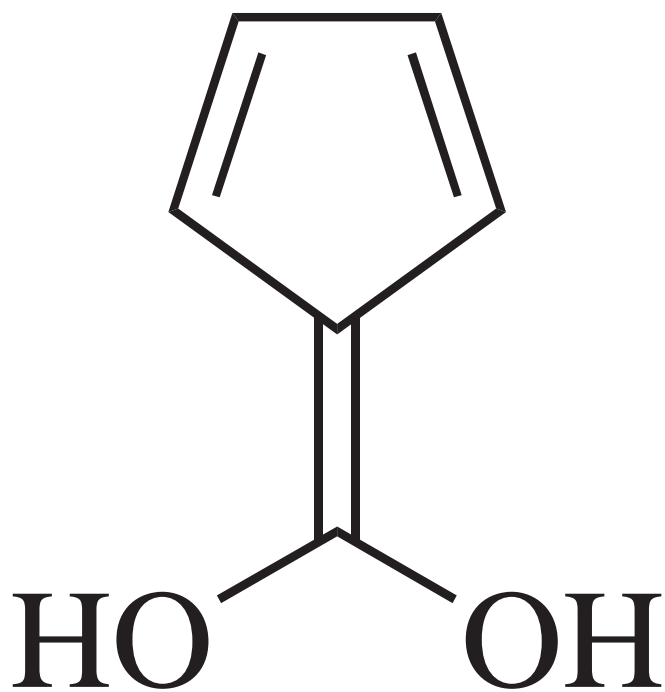
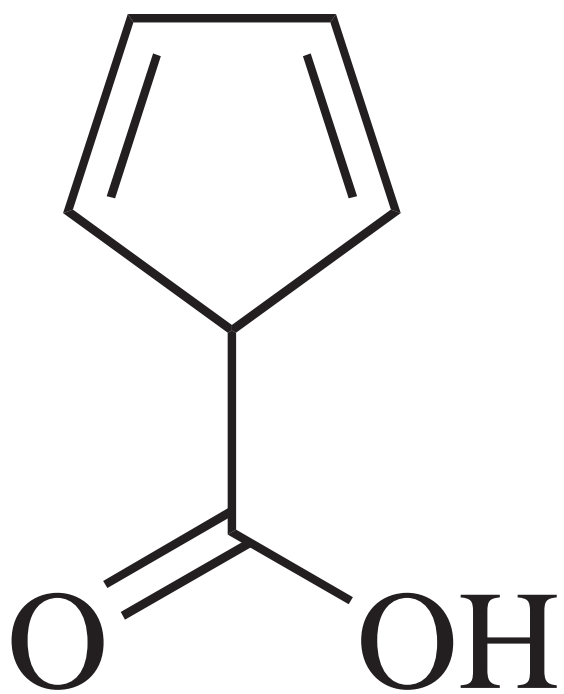


Figure 3
[Click here to download line figure: Fig. 3 eps.eps](#)

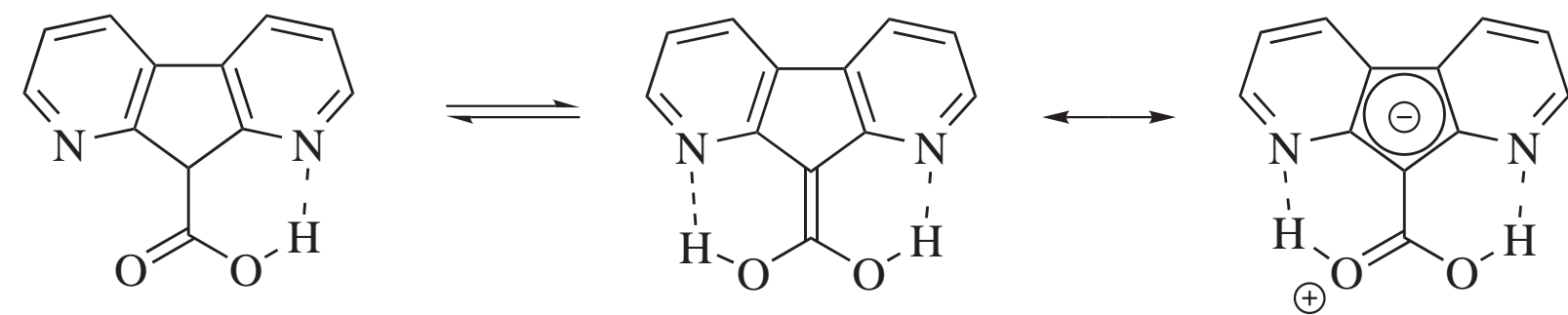


Figure 4
[Click here to download line figure: Fig. 4 eps.eps](#)

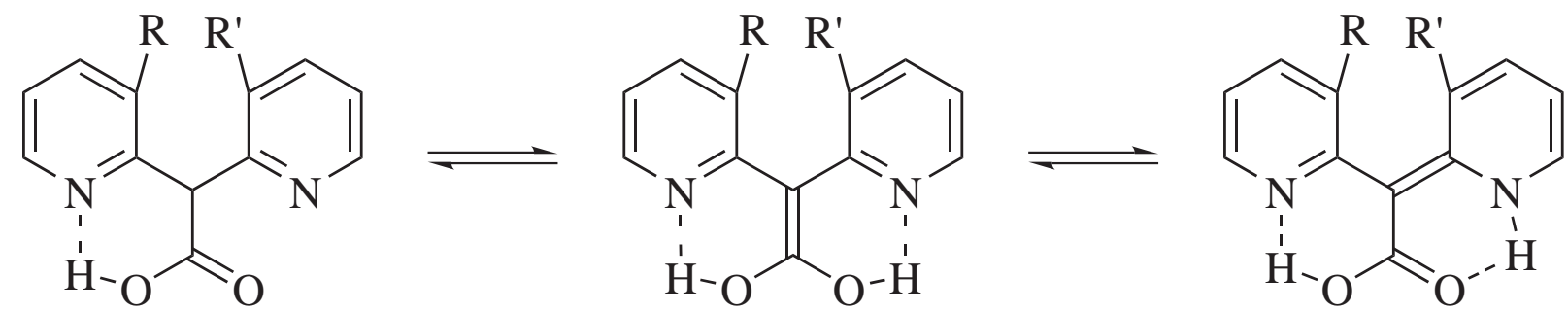
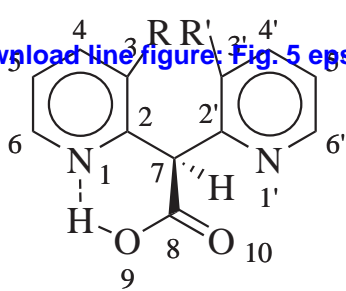
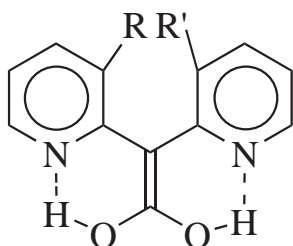


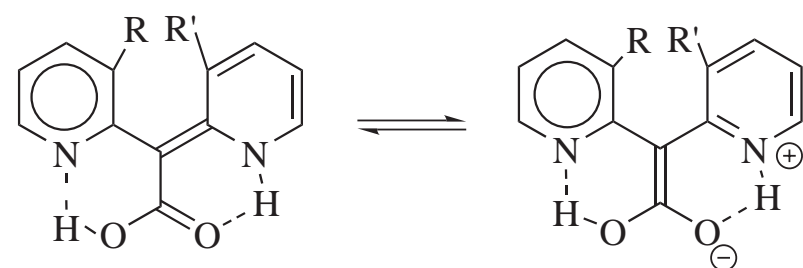
Figure 5
[Click here to download line figure: Fig. 5 eps.eps](#)



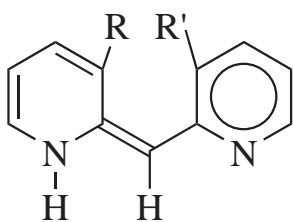
1a, b



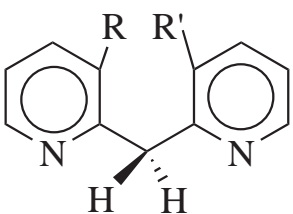
2a, b



3a, b



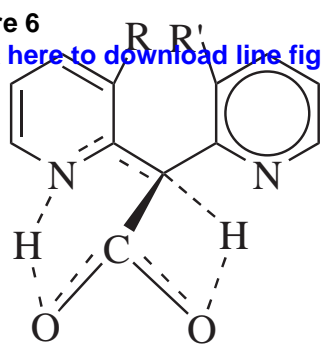
4a, b



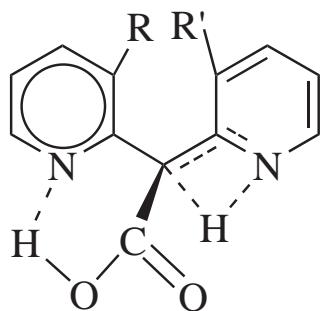
5a, b

R/R' = H/H (a) or none (b)

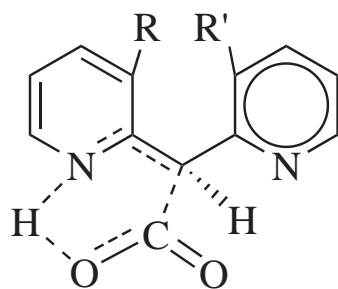
Figure 6
[Click here to download line figure: Fig. 6 eps.eps](#)



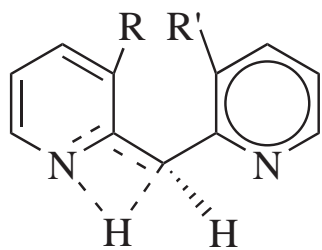
TS1a, b



TS2a, b



TS3a, b



TS4a, b

R/R' = H/H (a) or none (b)

Figure 7
[Click here to download high resolution image](#)

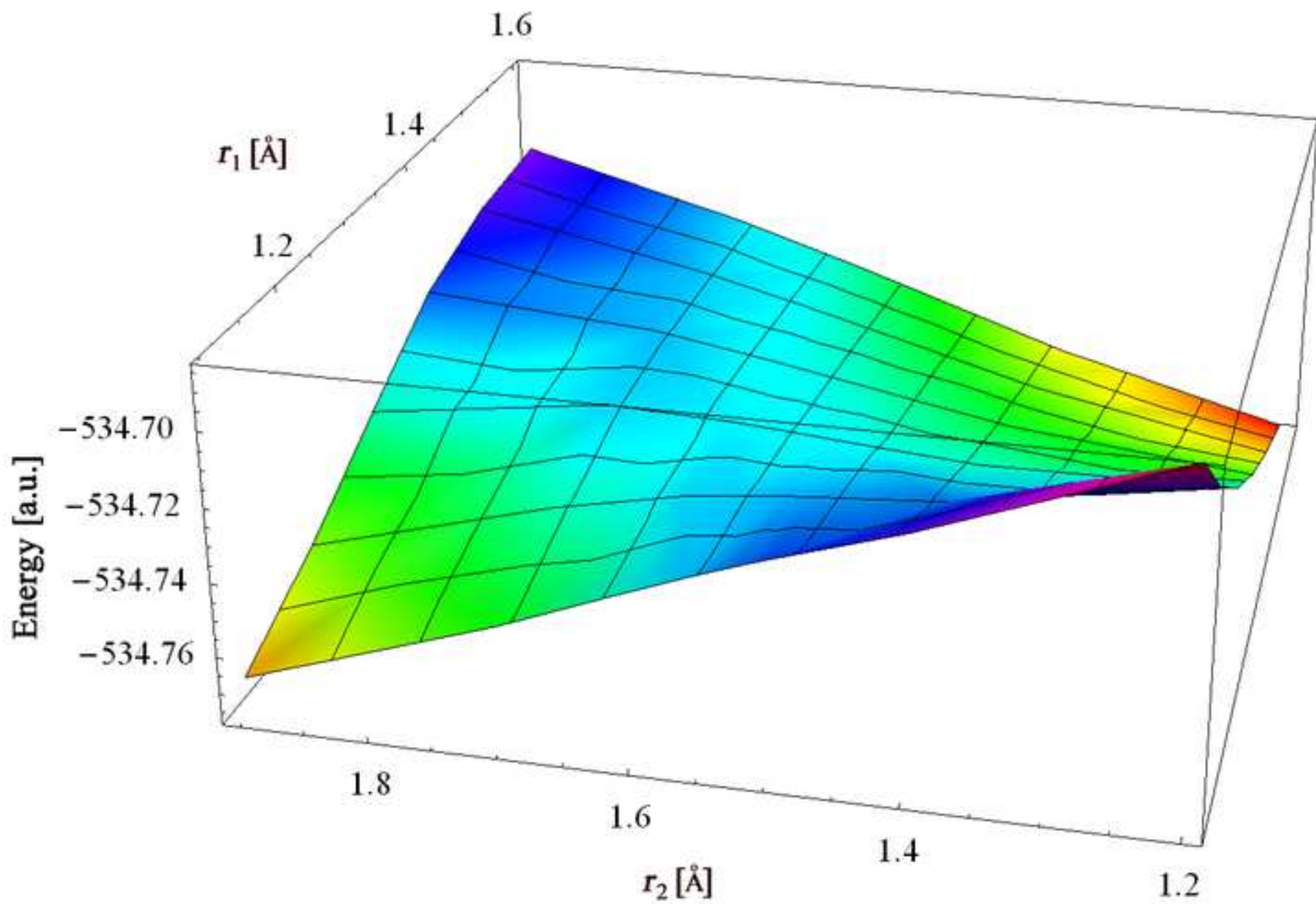


Figure 8_1a
[Click here to download high resolution image](#)

1a

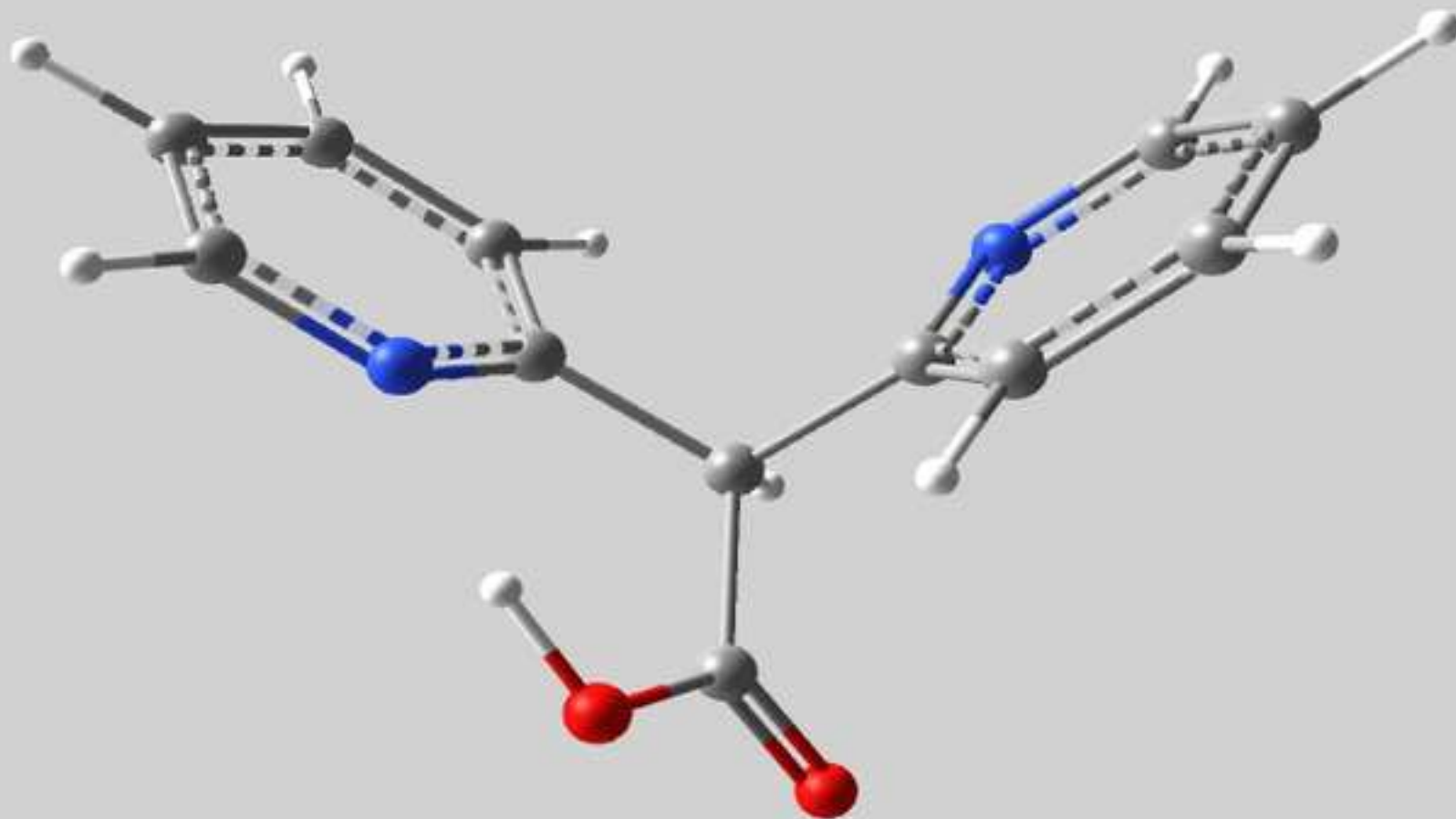


Figure 8_1b
[Click here to download high resolution image](#)

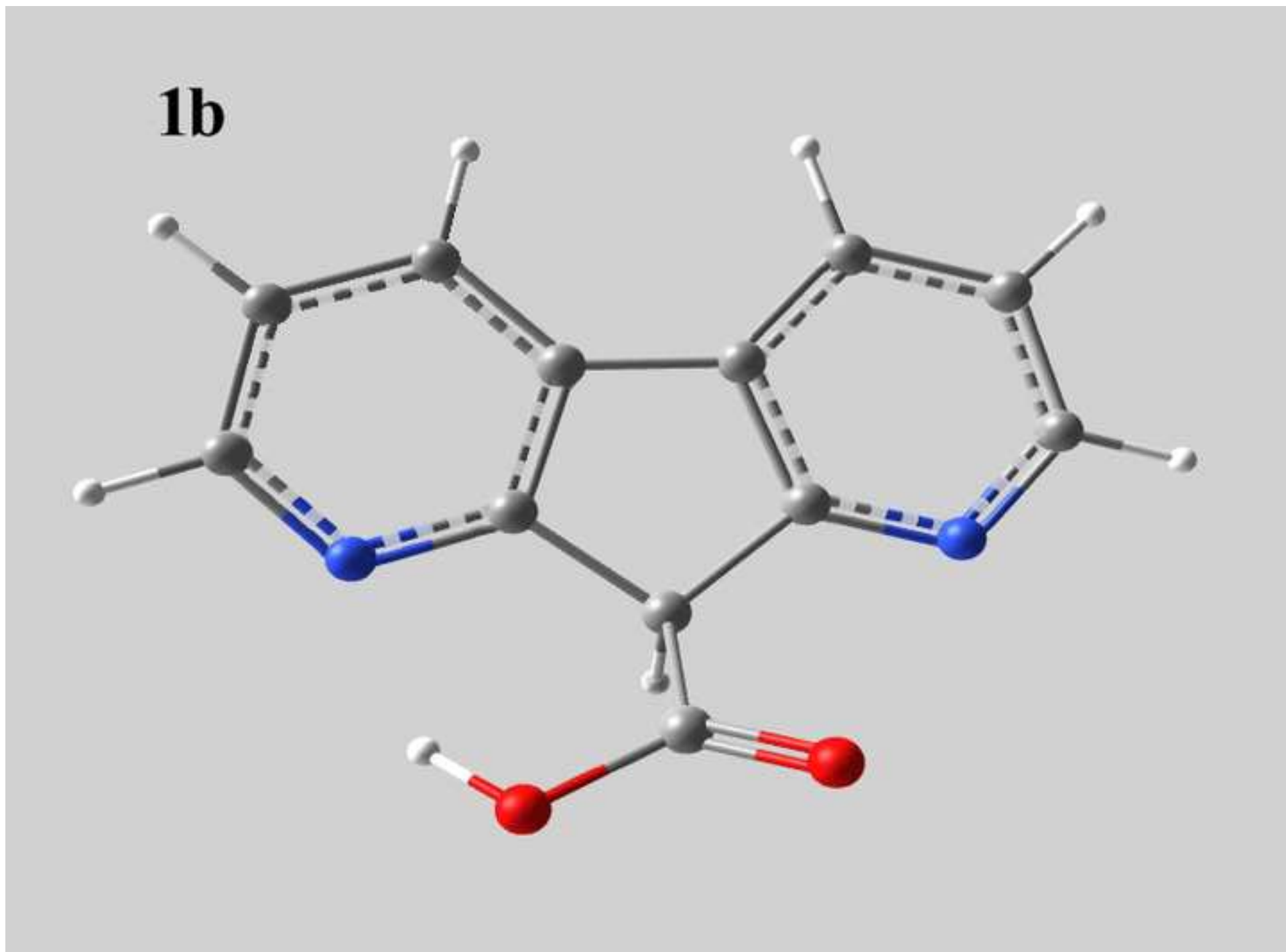


Figure 8_2a
[Click here to download high resolution image](#)

2a

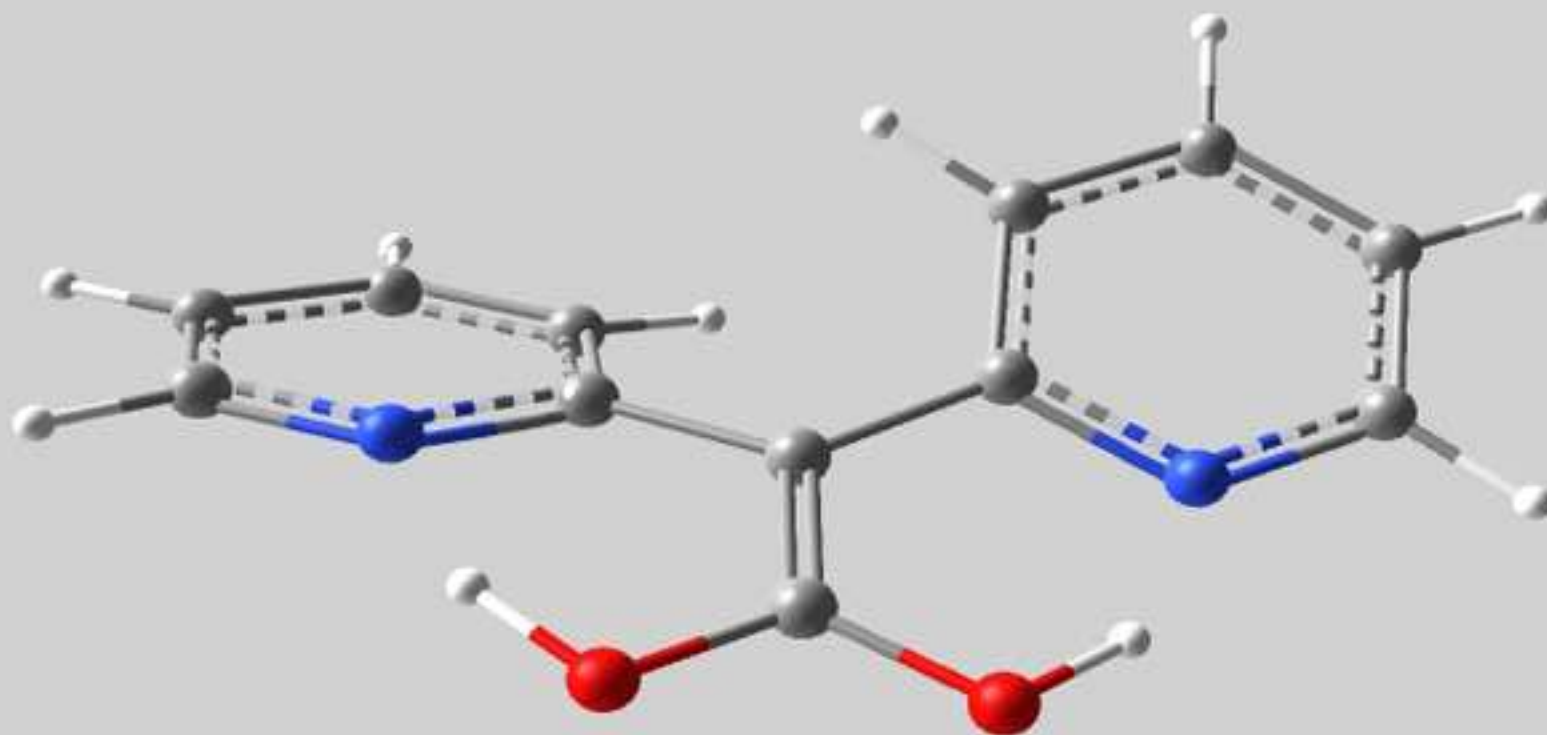


Figure 8_2b
[Click here to download high resolution image](#)

2b

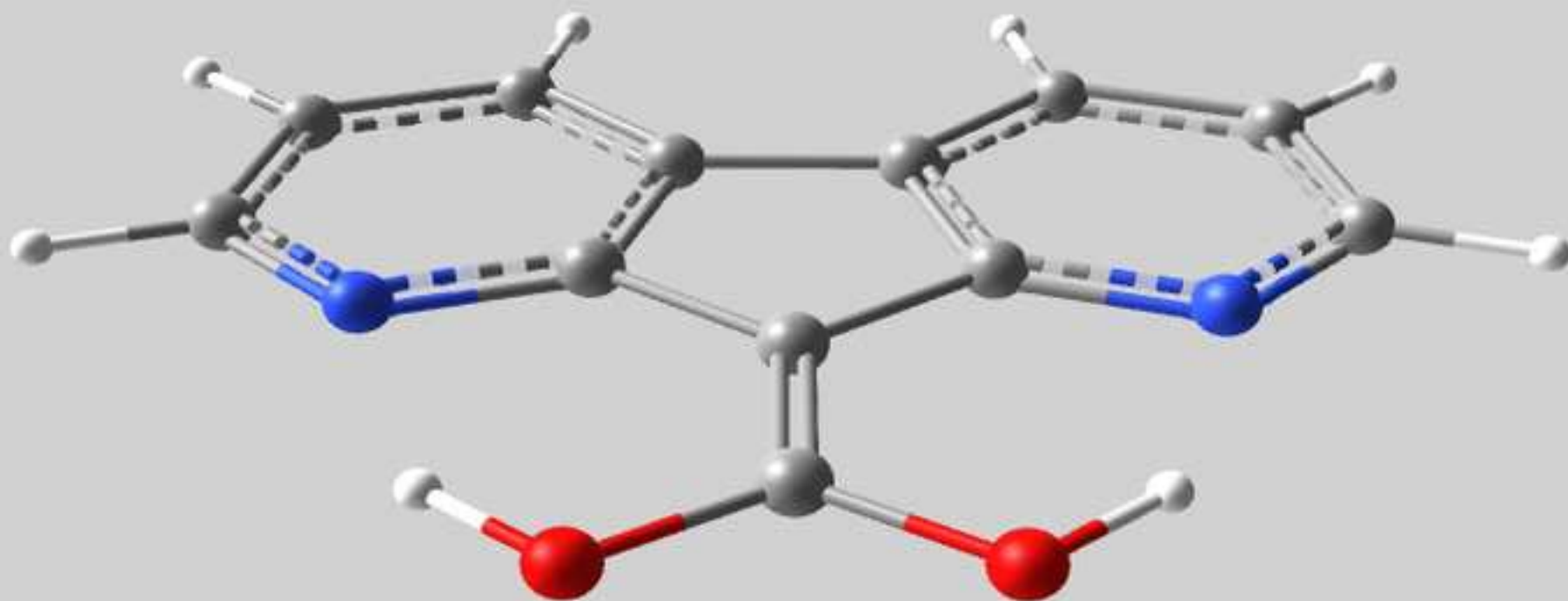


Figure 8_3a
[Click here to download high resolution image](#)

3a



Figure 8_3b
[Click here to download high resolution image](#)

3b

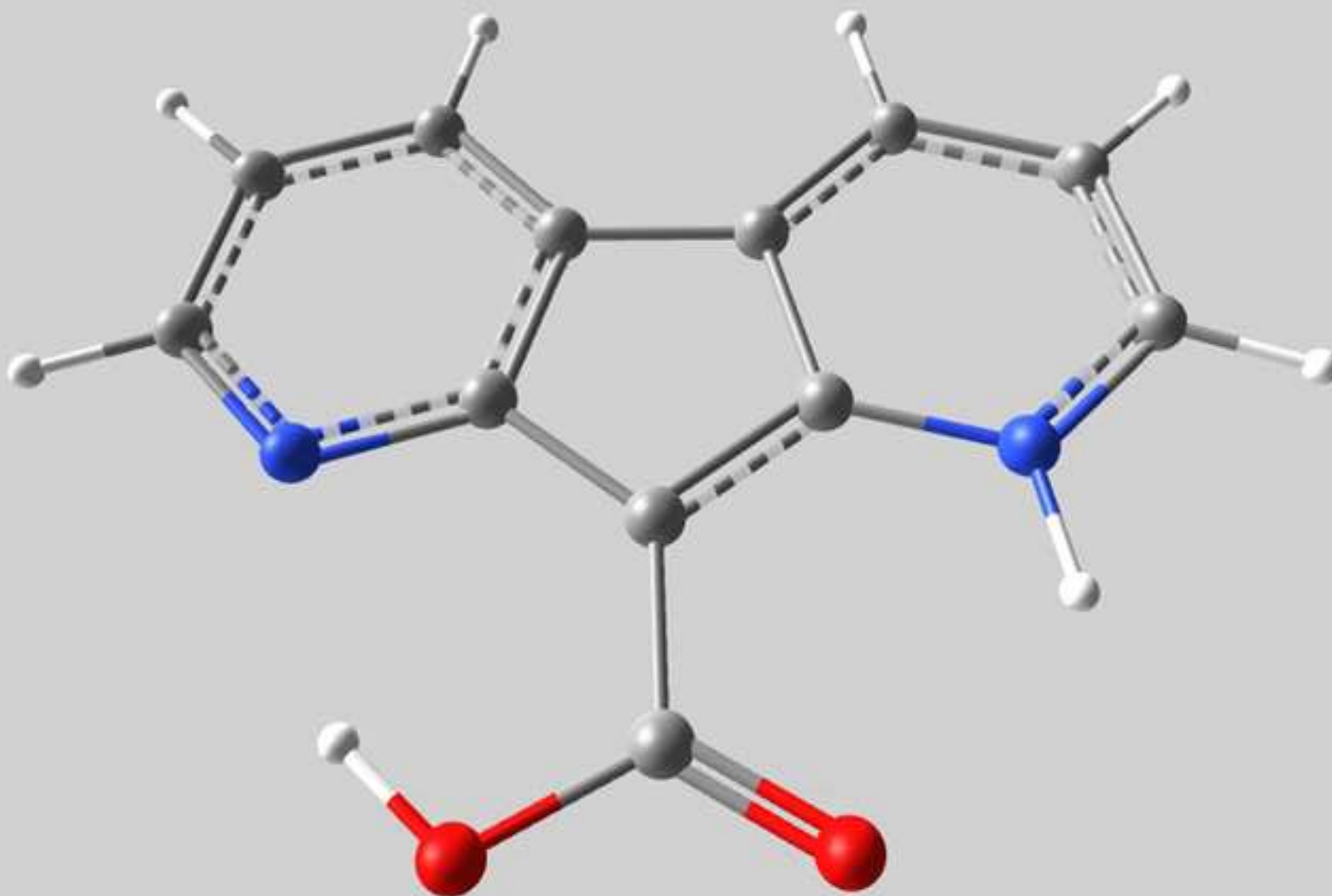


Figure 8_4a
[Click here to download high resolution image](#)

4a



Figure 8_4b
[Click here to download high resolution image](#)

4b

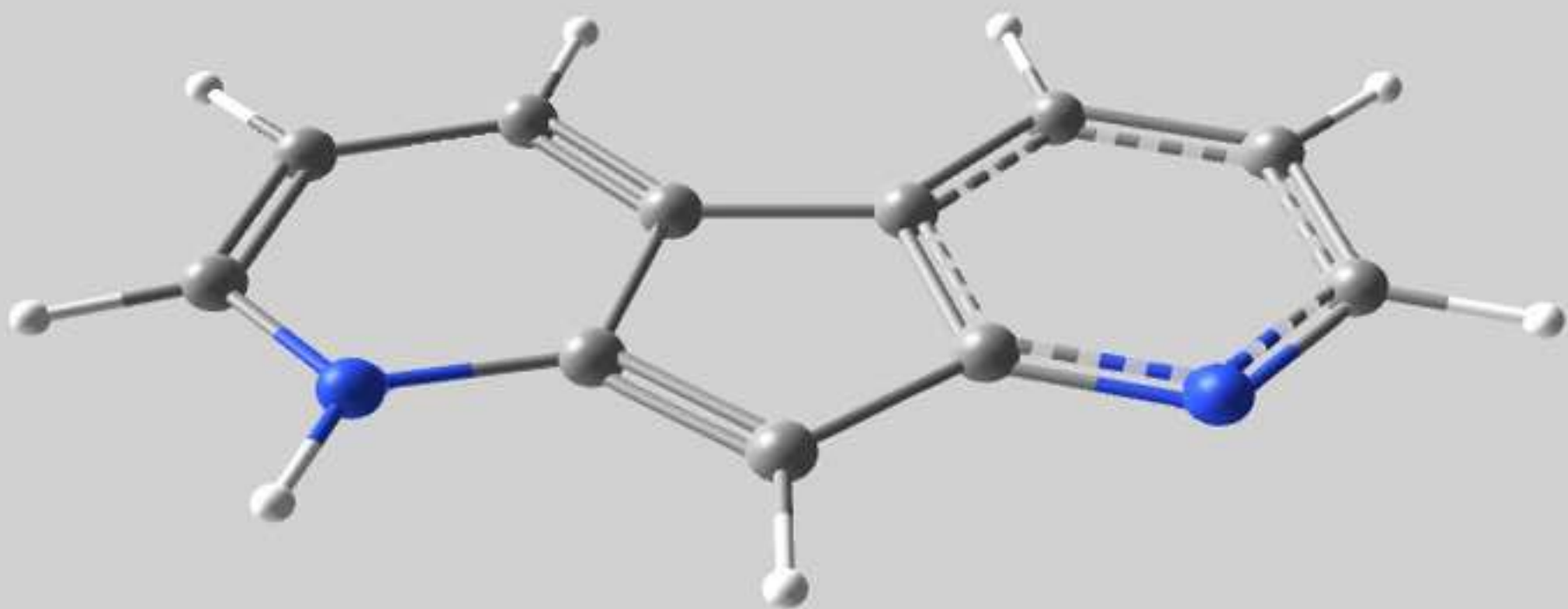


Figure 8_5a
[Click here to download high resolution image](#)

5a



Figure 8_5b
[Click here to download high resolution image](#)

5b

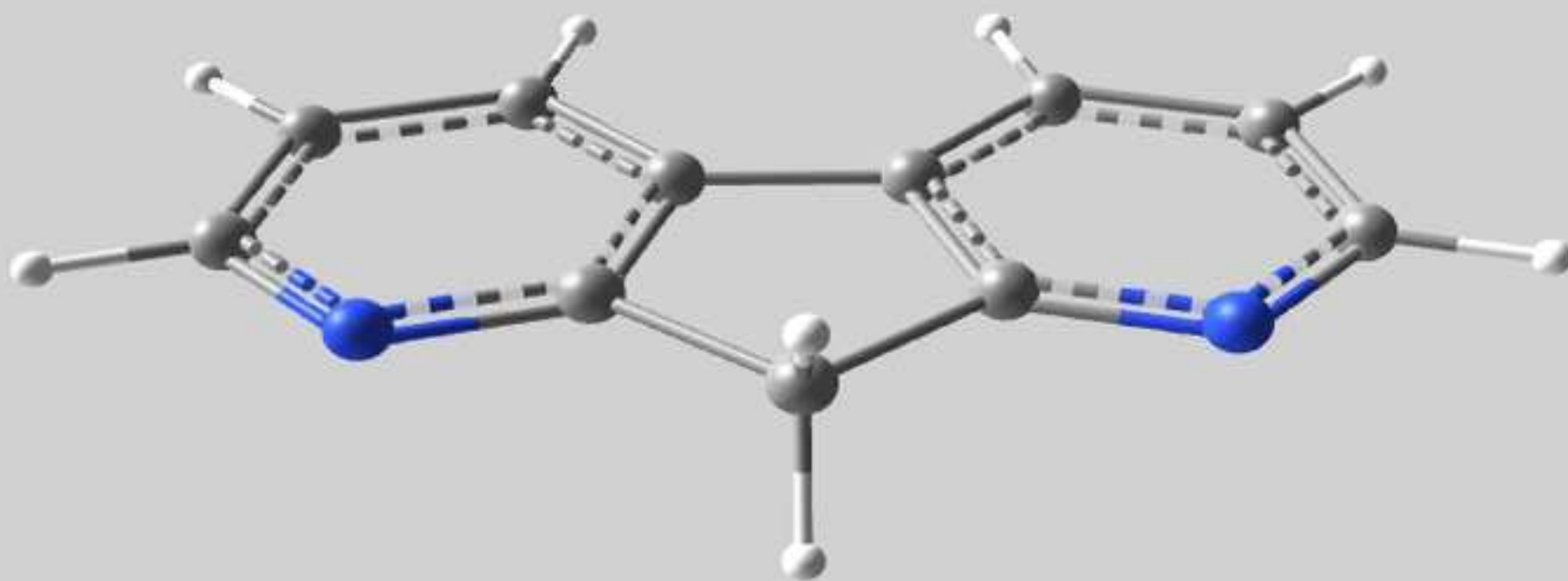


Figure 9
[Click here to download line figure: Fig. 9 eps.eps](#)

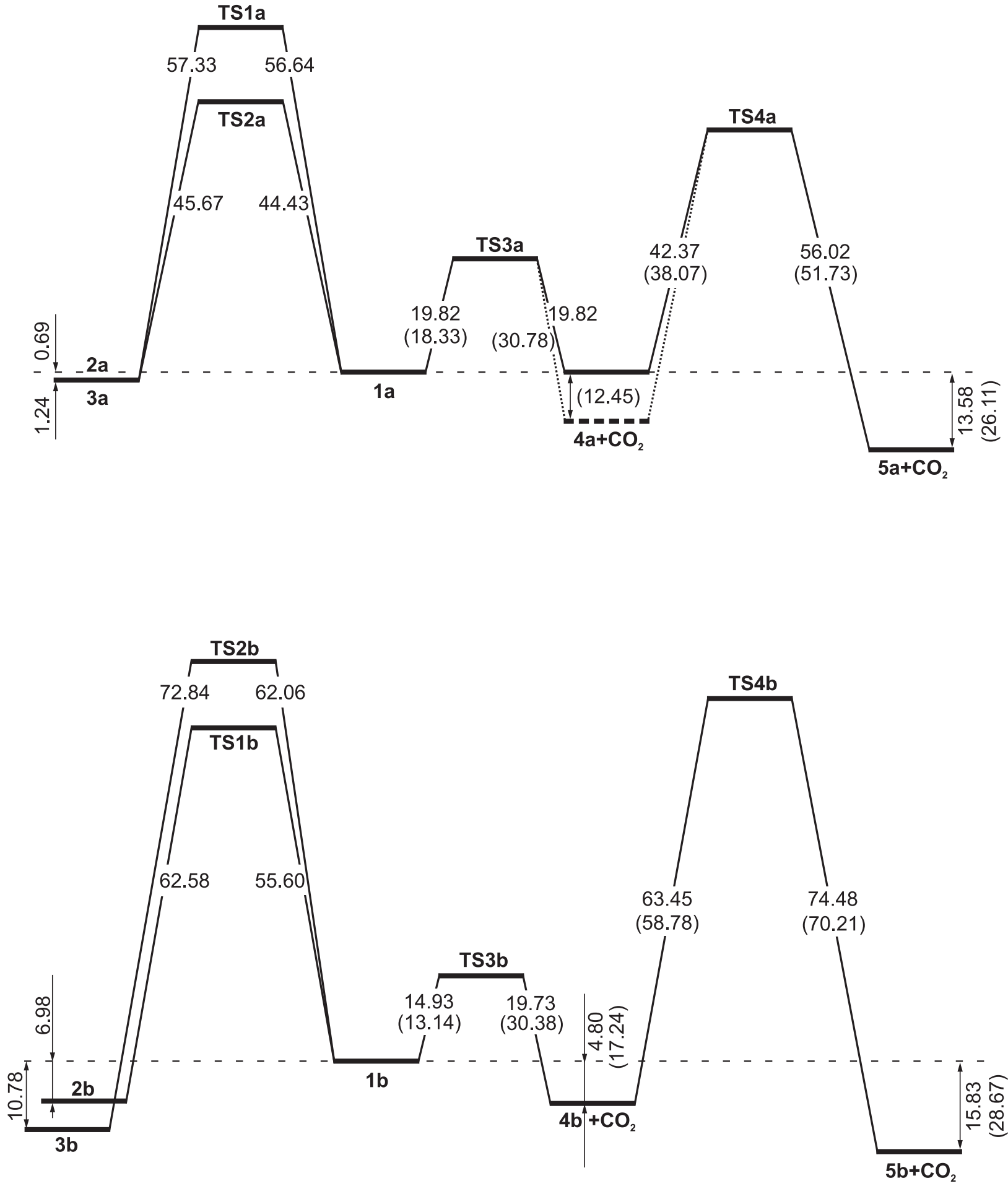


Figure 10
[Click here to download high resolution image](#)

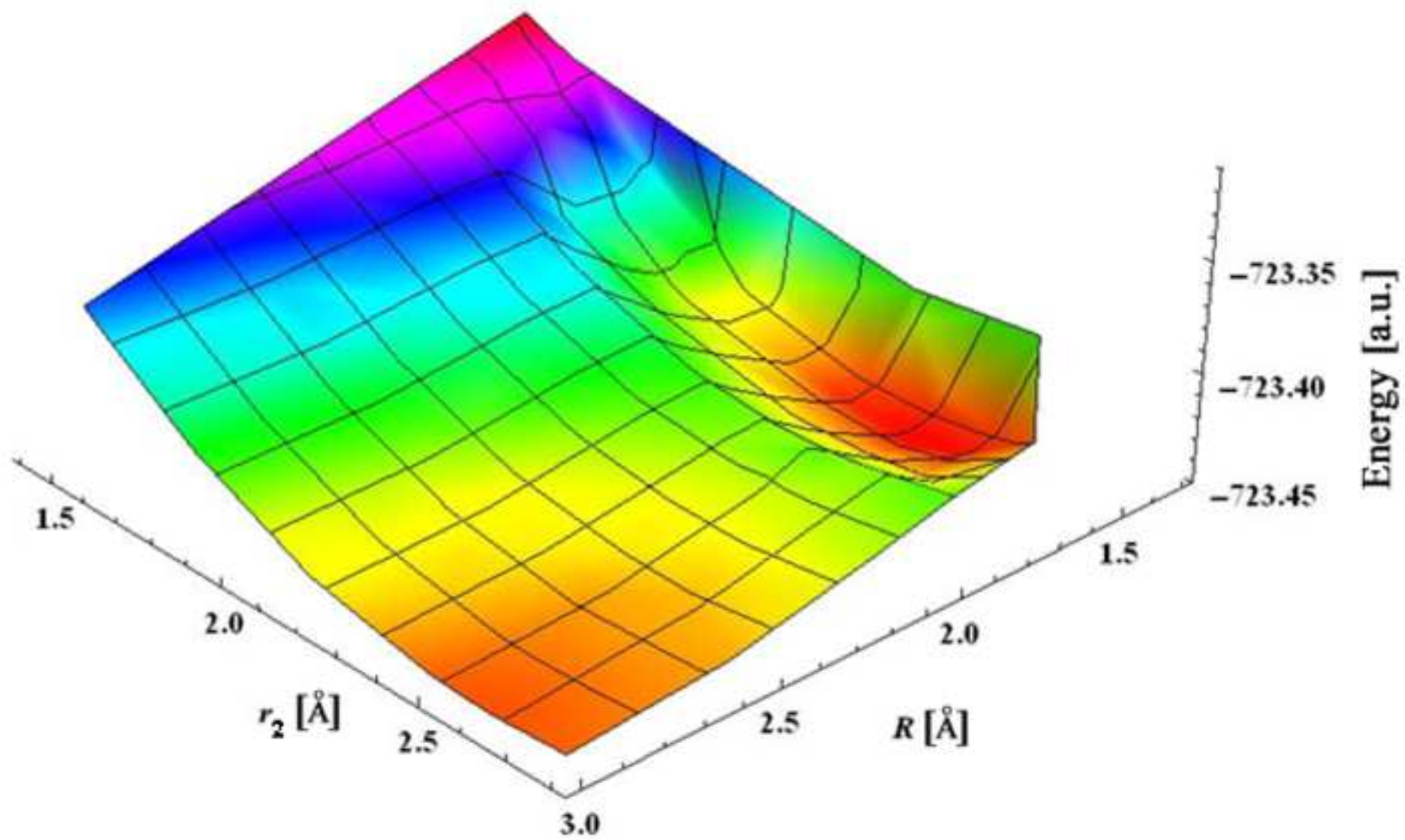


Figure 11a
[Click here to download high resolution image](#)

TS3a

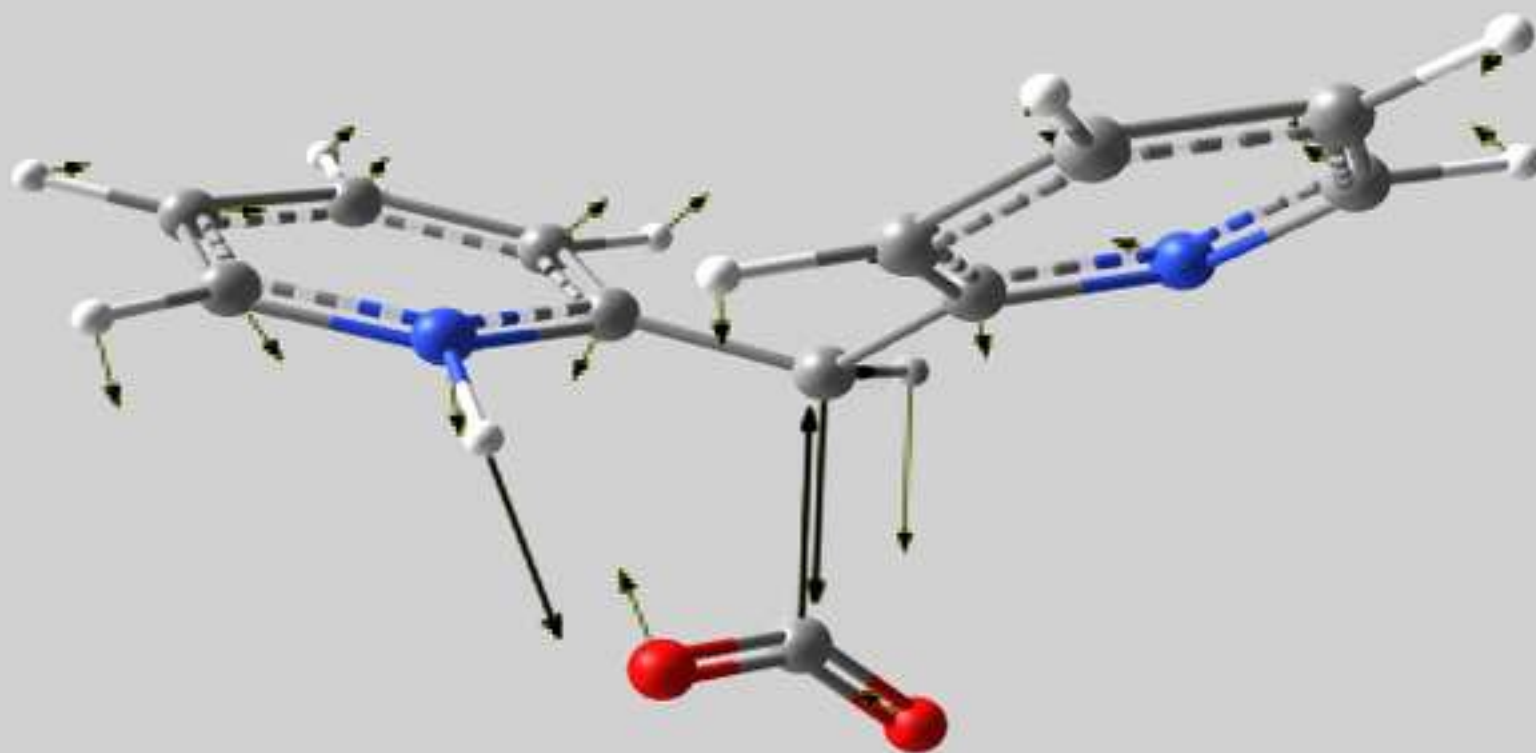


Figure 11b
[Click here to download high resolution image](#)

TS4a

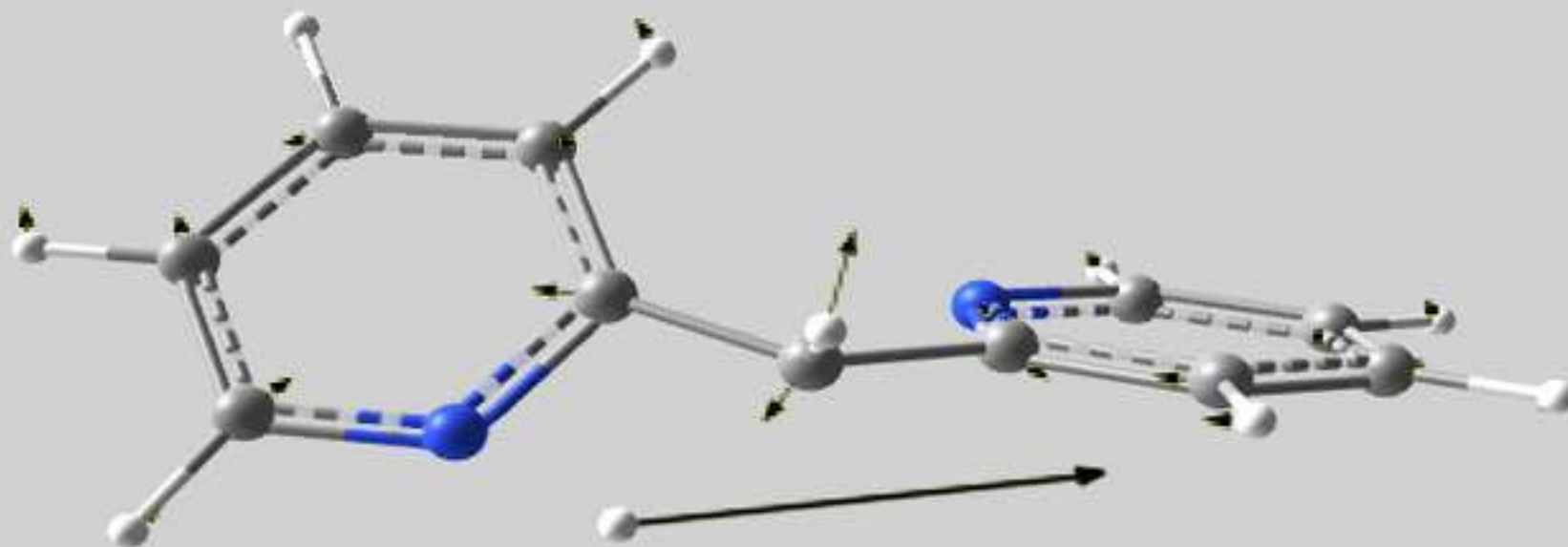


Figure 12a
[Click here to download high resolution image](#)

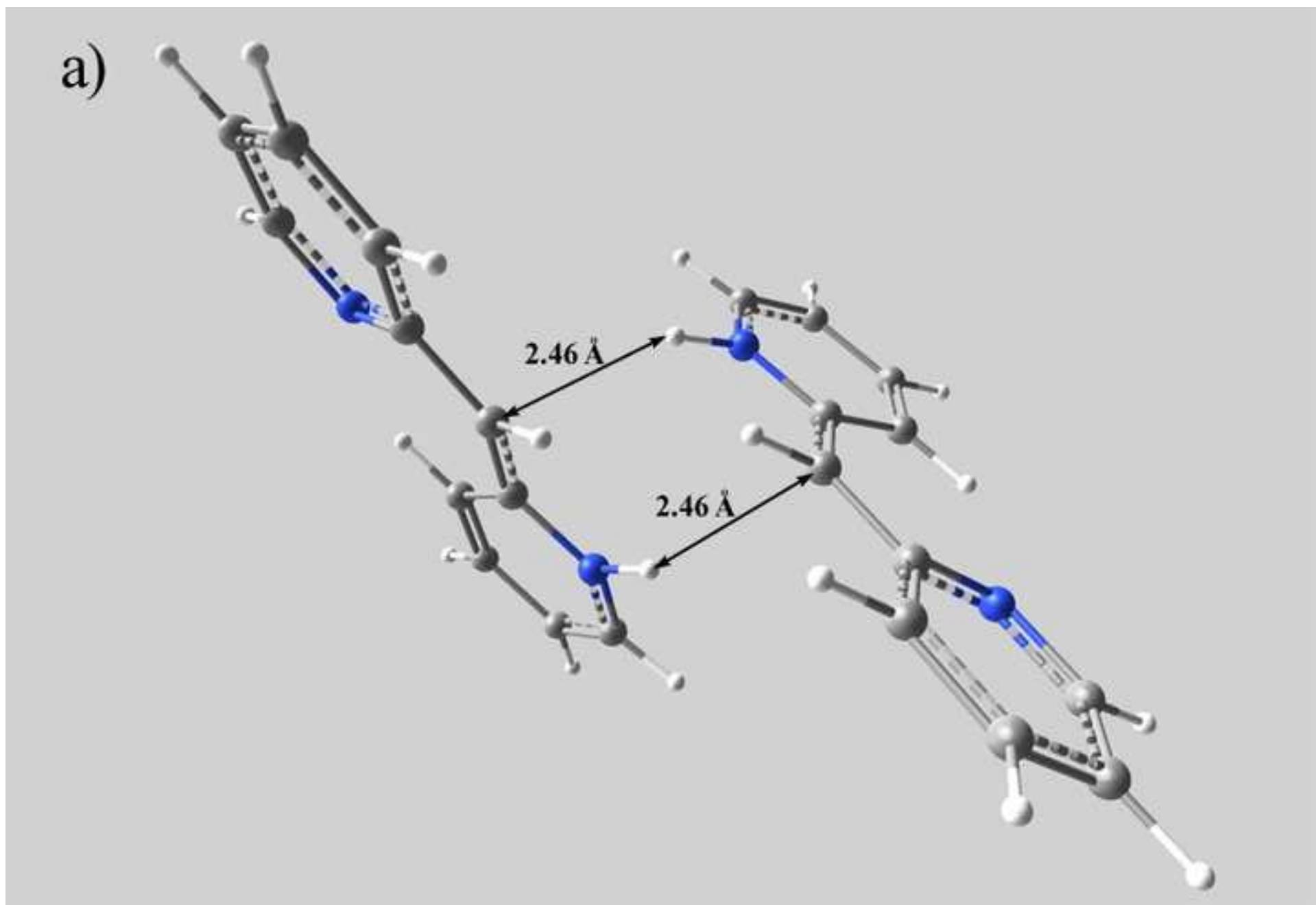


Figure 12b
[Click here to download high resolution image](#)

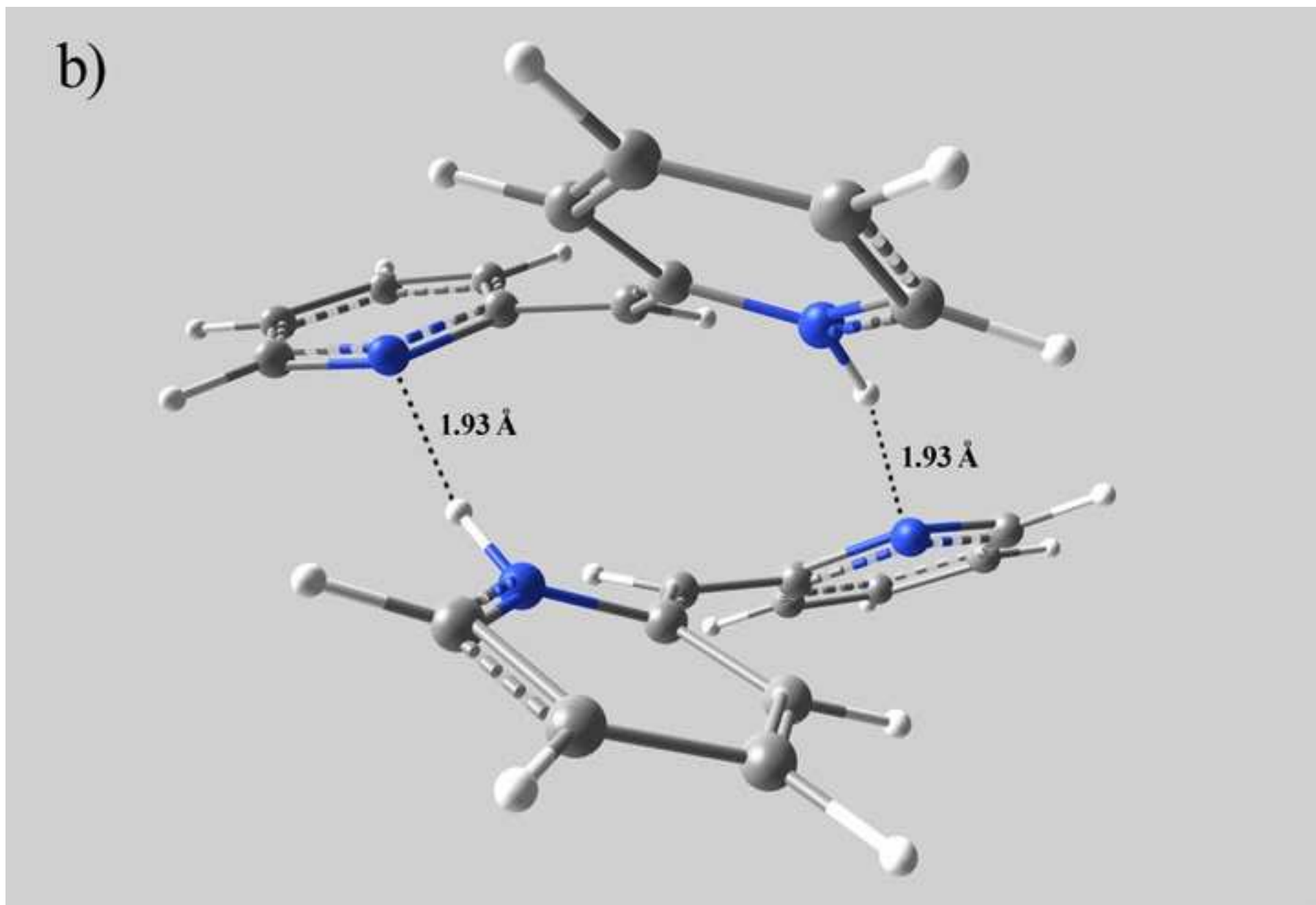


Figure 13a
[Click here to download high resolution image](#)

TS3b

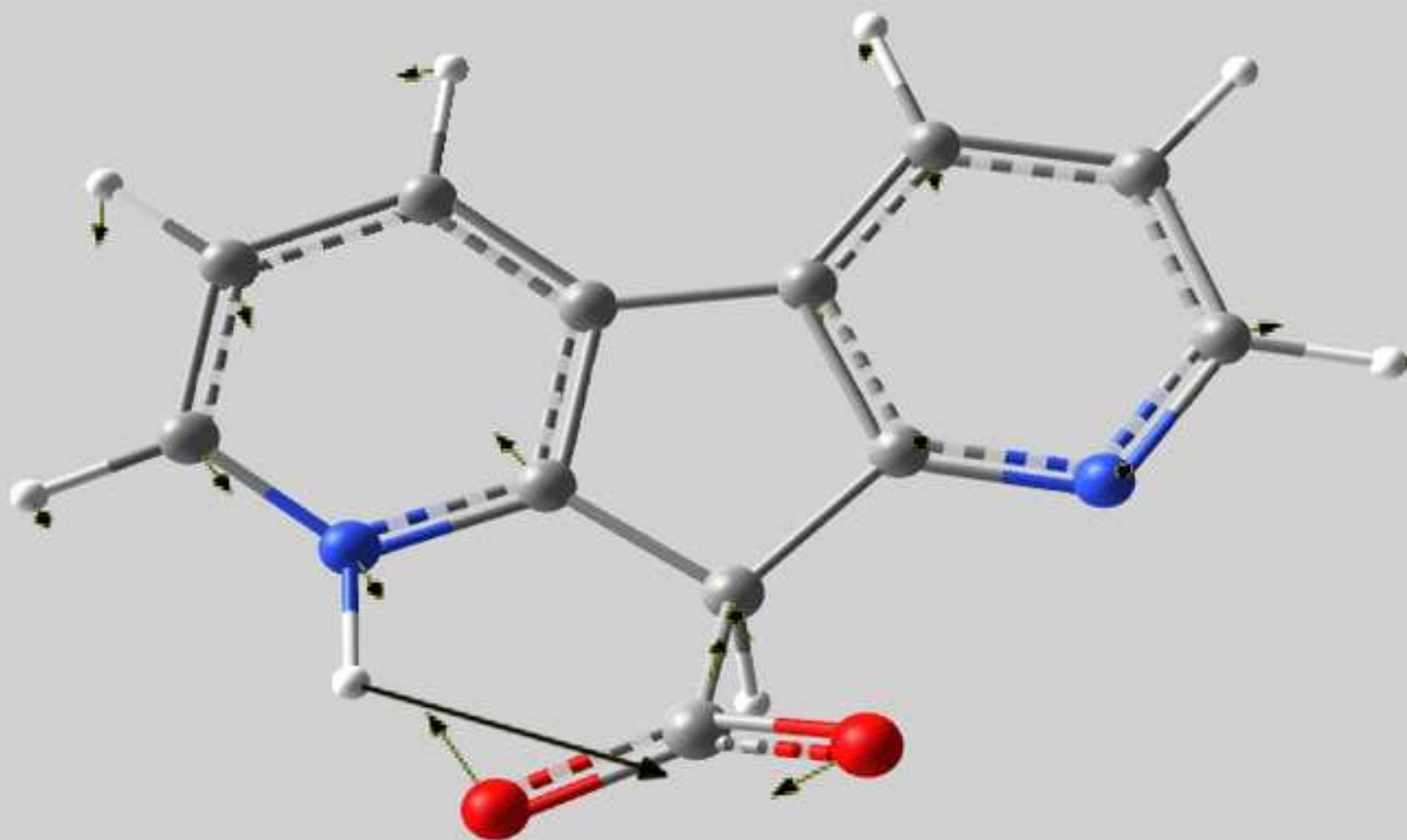


Figure 13b
[Click here to download high resolution image](#)

TS4b

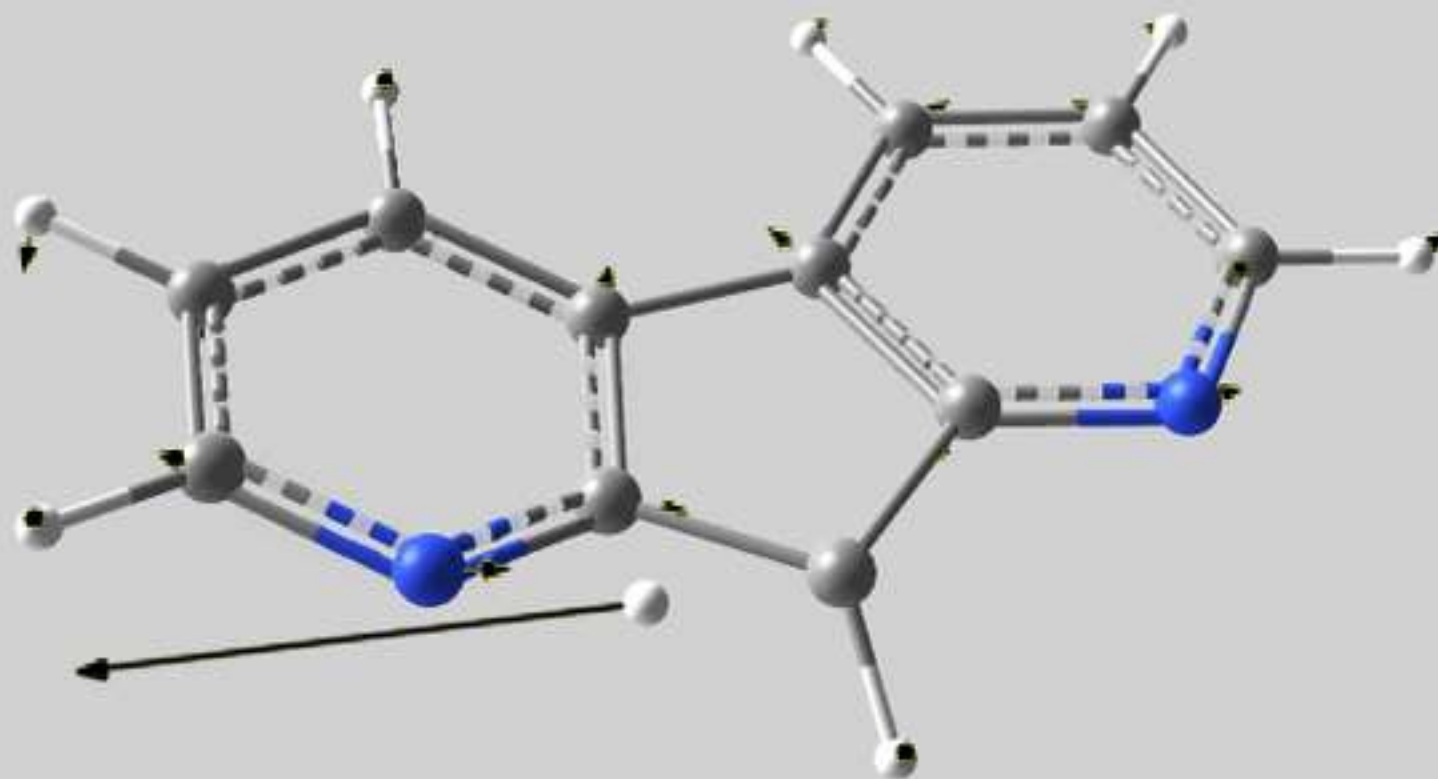


Figure 14
[Click here to download high resolution image](#)

